The Canadian Mineralogist
Vol. 46, pp. 1527-1554 (2008)
DOI : 10.3749/canmin.46.6.1527

THE CRYSTAL CHEMISTRY OF THE SCAPOLITE-GROUP MINERALS. I. CRYSTAL STRUCTURE AND LONG-RANGE ORDER

Elena SOKOLOVA[§] and Frank C. HAWTHORNE

Department of Geological Sciences, University of Manitoba, Winnipeg, Manitoba R3T 2N2, Canada

Abstract

Scapolite-group minerals are a group of rock-forming framework aluminosilicates common in a wide variety of igneous and metamorphic rocks. They have the general formula M_4 [T_{12} O_{24}] A, where M represents Na, K, Ca, Sr, Ba and Fe^{2+}, T stands for Si, Al, (Fe^{3+}), and A represents Cl, (CO_3), (SO_4). They constitute a non-binary solid-solution series involving the end members marialite (Na_4 [Al_3 Si_9 O_{24}] Cl, *Ma*) and meionite (Ca_4 [Al_6 Si_6 O_{24}] CO_3, *Me*). The crystal structures of eighteen scapolite-group minerals from $Me_{4.9}$ to $Me_{92.8}$ [$Me = 100\ \Sigma M^{2+} / \Sigma(M^{2+} + M^{+})$] have been refined with Mo$K\alpha$ X-radiation. The crystals, a 12.045–12.208, c 7.564–7.586 Å, V 1099.7–1130.1 Å^3, $I4/m$ or $P4_2/n$, $Z = 2$, were analyzed with an electron microprobe subsequently to collection of the X-ray intensity data. There are subtle differences between the behavior of the distinct T tetrahedra in the $I4/m$ and $P4_2/n$ structures. For Si and Al, determinative curves for the assignment of site populations from <T–O> distances were developed for each T site in each structure type, and T-site populations were assigned from these curves. In $I4/m$ marialite, there is no Al at the T(1) site. In $P4_2/n$ scapolite, Al is strongly ordered at T(2), and Si is strongly ordered at T(3), but this order is never complete. The A-site cation (Na, Ca, K) is [8]-coordinated in end-member marialite and is (on average) [8.5]-coordinated in end-member meionite. Each ($M\phi_n$) polyhedron shares two edges with adjacent ($M\phi_n$) polyhedra, forming a three-dimensional framework that interpenetrates the [$T_{12}O_{24}$] silicate framework. In (CO_3)-bearing structures, the model proposed by previous workers, four (CO_3) groups arranged about the 4 axis ($I4/m$) or $\bar{4}$ axis ($P4_2/m$), is consistent across the series from marialite to meionite. Any (SO_4) present is disordered by rotation of 90° about the central 4-fold axis; in $I4/m$ structures, each arrangement is 50% occupied, whereas in $P4_2/n$ structures, the occupancies of the two arrangements are not required to be equal.

Keywords: scapolite, marialite, meionite, crystal structure, electron-microprobe analysis, site populations, chlorine, carbonate, sulfate.

Sommaire

Les minéraux du groupe de la scapolite forment une famille d'aluminosilicates à trame répandus dans les roches ignées et métamorphiques. Dans leur formule générale, M_4 [T_{12} O_{24}] A, M représente Na, K, Ca, Sr, Ba et Fe^{2+}, T représente Si, Al, (Fe^{3+}), et A représente Cl, (CO_3) et (SO_4). Ils forment une solution solide non binaire entre les pôles marialite (Na_4 [Al_3 Si_9 O_{24}] Cl, *Ma*) et méionite (Ca_4 [Al_6 Si_6 O_{24}] CO_3, *Me*). Nous avons affiné la structure cristalline de dix-huit membres de la série allant de $Me_{4.9}$ à $Me_{92.8}$ [$Me = 100\ \Sigma M^{2+} / \Sigma(M^{2+} + M^{+})$] par diffraction X avec rayonnement Mo$K\alpha$. Par la suite, nous avons analysé ces cristaux, a 12.045–12.208, c 7.564–7.586 Å, V 1099.7–1130.1 Å^3, $I4/m$ ou $P4_2/n$, $Z = 2$, avec une microsonde électronique. Nous signalons la présence de légères différences dans le comportement des tétraèdres entre les structures $I4/m$ et les structures $P4_2/n$. Pour Si et Al, des courbes utilisées pour assigner la population des sites à partir des distances <T–O> ont été développées pour chaque site T dans chaque type de structure, et les populations aux sites T ont été assignées en fonction de ces courbes. Dans la marialite $I4/m$, il n'y a pas de Al dans le site T(1). Dans la scapolite $P4_2/n$, l'aluminium est fortement concentré sur le site T(2), et le Si est fortement ordonné sur le site T(3), mais cette mise en ordre demeure incomplète. Le cation sur le site A (Na, Ca, K) possède une coordinence [8] dans le pôle marialite et, en moyenne, [8.5] dans le pôle méionite. Chaque polyèdre ($M\phi_n$) partage deux arêtes avec des polyèdres ($M\phi_n$) adjacents, pour former une trame tridimensionnelle qui interpénêtre la trame de tétraèdres [$T_{12}O_{24}$]. Dans les structures contenant le (CO_3), le modèle proposé antérieurement, avec quatre groupes (CO_3) disposés autour de l'axe 4 ($I4/m$) ou $\bar{4}$ ($P4_2/m$), s'applique sur toute la série, de marialite à méionite. Là où des groupes (SO_4) sont présents, ils sont désordonnés par rotation de 90° par rapport à l'axe central d'ordre 4; dans les structures $I4/m$, chaque arrangement a une occupation de 50%, tandis que dans les structures $P4_2/n$, les taux d'occupation des deux arrangements ne sont pas nécéssairement égaux.

(Traduit par la Rédaction)

Mots-clés: scapolite, marialite, méionite, structure cristalline, analyse avec microsonde électronique, populations des sites, chlore, carbonate, sulfate.

[§] *E-mail address*: elena_sokolova@umanitoba.ca

INTRODUCTION

The scapolite group of rock-forming framework aluminosilicates is common in a wide variety of igneous and metamorphic rocks. These minerals have the general formula

$M_4\ [T_{12}\ O_{24}]\ A$

where M represents Na, K, Ca, Sr, Ba and Fe^{2+}, T stands for Si, Al, (Fe^{3+}), and A represents Cl, (CO_3), (SO_4) + minor Br. They constitute a non-binary solid-solution series involving the end members marialite ($Na_4\ [Al_3\ Si_9\ O_{24}]\ Cl$, *Ma*) and meionite ($Ca_4\ [Al_6\ Si_6\ O_{24}]\ CO_3$, *Me*). Shaw (1960a, b) proposed the percentage of meionite [$Me\ \% = 100\ Ca\ /\ (Na + Ca)$] as the chemical index to indicate the composition of scapolite; currently, the meionite percentage [$Me\ \% = 100\ \Sigma M^{2+}\ /\ \Sigma(M^{2+} + M^{+})$] is commonly used (*e.g.*, Teertstra & Sherriff 1996, 1997). For a century, only two mineral species, marialite and meionite, were known (Bayliss 1987). Silvialite, ideally $Ca_4\ [Al_6\ Si_6\ O_{24}]\ SO_4$, the S-dominant member of the scapolite group, was described by Teertstra *et al.* (1999). There has been considerable recent work on the crystal structure and crystal chemistry of the scapolite-group minerals by Rietveld structure refinement and MAS NMR (Magic-Angle Spinning Nuclear Magnetic Resonance) spectroscopy (Sokolova *et al.* 1996, 2000, Sherriff *et al.* 1998, 2000), and HRTEM (High-Resolution Transmission Electron Microscopy) (Seto *et al.* 2004). However, major questions remain concerning the nonlinear variation in chemical composition, variation in Al–Si order, and changes in space group across the marialite–meionite series. These questions are answered in these two papers: in the first paper, we focus on experimentally deriving accurate site-populations, and in the second, we address the major questions outlined above.

It is general practice to denote the chemical composition of scapolite by the *Me* content [Me_x, $x \equiv 100\ Ca\ /\ (Na + Ca)$]. This symbolism is formally not correct: marialite–meionite is not a binary solid-solution series, and hence it is not suitable to represent chemical variation by a symbol that would normally represent the amount of that specific end-member in the composition under consideration. However, Me_x is a convenient symbol to use (provided we recognize that it represents only the amount of Ca in the structure) in view of the fact that it is embedded in the literature on the scapolite-group minerals.

PREVIOUS WORK

Structure topology

The first model for the crystal structure of scapolite was proposed by Pauling (1930) and Schiebold & Seumel (1932). Papike & Zoltai (1965), Papike & Stephenson (1966), Lin & Burley (1973a,b,c, 1975), Ulbrich (1973a), Levien & Papike (1976), Peterson *et al.* (1979) and Aitken *et al.* (1984) confirmed the original model of Pauling (1930), established two space groups for scapolite, $I4/m$ and $P4_2/n$, and covered the compositional range $Me_{19–94}$. Comodi *et al.* (1990), Belokoneva *et al.* (1991, 1993) and Sokolova *et al.* (2000) added further structural data, and the crystal structure of silvialite was refined by Teertstra *et al.* (1999). A study of structural parameters and cation order using Rietveld structure refinement and MAS NMR spectroscopy was done for 15 scapolite samples in the range $Me_{0.2–99.7}$ (Sokolova *et al.* 1996, Sherriff *et al.* 1998, 2000).

The crystal structure of scapolite can occur in two space groups, $I4/m$ and $P4_2/n$. There are two [$T(1)$ and $T(2)$ in $I4/m$] and three [$T(1)$, $T(2)$ and $T(3)$ in $P4_2/n$] tetrahedrally coordinated T sites. At the $I4/m \rightarrow P4_2/n$ transition, the $T(2)$ site splits into the $T(2)$ and $T(3)$ sites (Table 1). There is one unique M site in both space groups, occupied primarily by Na and Ca. The M cation is [8]-coordinated by seven framework O atoms and one Cl atom in marialite, and [8]- and [9]-coordinated by seven framework O atoms and one or two O atoms of the (CO_3) group in meionite. There is one unique A site occupied primarily by Cl, (CO_3) and (SO_4).

There are two types of four-membered rings of tetrahedra. The type-1 ring consists of $T(1)$ tetrahedra with their apices pointing in the same direction along the c axis. In the type-2 ring, the apices of the $T(2)$ tetrahedra point alternately up and down c. In the space group $P4_2/n$, the type-2 ring consists of $T(2)$ and $T(3)$ tetrahedra, each with an equipoint rank of 8. In the space group $I4/m$, the $T(2)$ and $T(3)$ tetrahedra combine to give rise to the $T(2)$ site with an equipoint rank of 16. Rings of two types form a framework (Figs. 1a, b) with interstitial sites occupied by M cations and A anions. The two types of rings form five-membered rings that are stacked

TABLE 1. SITE SPLITTING AT THE $I4/m \rightarrow P4_2/n$ TRANSITION

$I4/m$			$P4_2/n$		
Site	Wyckoff symbol	Symmetry	Site	Wyckoff symbol	Symmetry
$T(1)$	8h	m	$T(1)$	8g	1
$T(2)$	16l	1	$T(2)$	8g	1
			$T(3)$	8g	1
M	8h	m	M	8g	1
A	2b	$4/m$	A	2b	$\bar{4}$
O(1)	8h	m	O(1)	8g	1
O(2)	8h	m	O(2)	8g	1
O(3)	16l	1	O(3)	8g	1
			O(4)	8g	1
O(4)	16l	1	O(5)	8g	1
			O(6)	8g	1
O(7)	8h	m	O(7)	8g	1
O(8)	8h	m	O(8)	8g	1
O(9)	8h	m	O(9)	8g	1
O(10)	16l	1	O(10)	8g	1
			O(11)	8g	1

along *c* (Figs. 2a, b). The type-1 rings and columns built of type-2 rings link to form a cage that contains the *A* site. The point symmetry of the *A* site is $4/m$ or $\bar{4}$, and each *A* site is surrounded by four *M* sites. Both these symmetries are in accord with occupancy of the *A* site by Cl. However, where the *A* site is "occupied" by (CO_3), the point symmetry of the (CO_3) group is not in accord with the point symmetries of the *A* site in either space group, and hence the (CO_3) group is disordered in the scapolite structure (Papike & Stephenson 1966, Levien & Papike 1976, Aitken *et al.* 1984). Where the *A* site is "occupied" by (SO_4), the point symmetry of the (SO_4) group, $\bar{4}$, is in accord with the point symmetry of the *A* site in the space group $P4_2/n$ but not in the space group $I4/m$. Peterson *et al.* (1979) showed that the (SO_4) groups are centered at (000) in two orientations related by a 90° rotation about the $\bar{4}$ axis.

Expansion or contraction of the structure occurs by coupled rotation of the four-membered rings. This effect was described as a function of composition by Papike & Stephenson (1966), as a function of temperature by Levien & Papike (1976) and Graziani & Lucchesi (1982), and as a function of pressure by Comodi *et al.* (1990).

Si–Al order

The principal structural difference between the $I4/m$ and $P4_2/n$ structures involves differences in Al–Si order in the framework of tetrahedra. In end-member marialite (Me_0), *T*(1) is occupied completely by Si, and *T*(2) is occupied by (5 Si + 3 Al) / 8 (Lin & Burley 1973a). With increasing Al content, Al first enters the *T*(2) site, and then the *T*(1) site. With change in symmetry from $I4/m$ to $P4_2/n$, the *T*(2) site splits into two sites, *T*(2) and *T*(3), with Al slightly to strongly ordered at *T*(2). There have been several proposals for various completely ordered Al–Si arrangements at specific compositions, but as we show here, none of them are correct, and we will not review them here.

THE MARIALITE–MEIONITE SOLID-SOLUTION

Evans *et al.* (1969) proposed two mechanisms of substitution in scapolite: (1) between Me_0 and Me_{75}, the substitution is $Na_3 + Si_2 + Cl \rightleftarrows Ca_3 + Al_2 + (CO_3)$; (2) between Me_{75} and Me_{100}, the substitution is $Na + Si \rightleftarrows Ca + Al$ (as in plagioclase feldspars). In this scheme, the *A* site is ideally filled with $(CO_3)^{2-}$ from Me_{75} to Me_{100}. This scheme has been interpreted as evidence for two binary solid-solution series that meet at Me_{75} (Ulbrich 1973b). Aitken *et al.* (1984) suggested the presence of two series because of the change in space group at approximately Me_{75}.

Until the 1990s, detailed work focused on the more abundant Ca-rich scapolites, presumably because (NaCl)-rich scapolite is quite uncommon. Lieftink *et al.* (1993) and Zolotarev (1993) reported the occurrence of (NaCl)-rich scapolites close to end-member marialite. Sherriff & Teertstra (1994) reviewed available chemical data for scapolite-group minerals and concluded that (NaCl)-rich scapolite does not follow the substitution $Na + Si \rightleftarrows Ca + Al$. Zolotarev (1996) proposed three subseries in scapolite based on discontinuities in the variation of the *c* dimension with variation in *Me* content:

(A): $Na_4\,[Al_3\,Si_9\,O_{24}]\,Cl$ (*Ma*) –
$Ca\,Na_3\,[Al_4\,Si_8\,O_{24}]\,Cl$;

(B): $Ca\,Na_3\,[Al_4\,Si_8\,O_{24}]\,Cl$ –
$Na\,Ca_3\,[Al_5\,Si_7\,O_{24}]\,(CO_3)$;

(C): $Na\,Ca_3\,[Al_5\,Si_7\,O_{24}]\,(CO_3)$ –
$Ca_4\,[Al_6\,Si_6\,O_{24}]\,(CO_3)$ (Me_{100}).

The A–B boundary is at $Me_{20–25}$, and the B–C boundary is at $Me_{60–67}$. Teertstra & Sherriff (1996, 1997) also proposed three subseries based on discontinuities in cell dimensions as a fraction of Al content, which they also associated with changes in space group. The boundaries between these series are located at 3.6 and 4.7 Al *apfu*, and are fairly similar to the subdivisions of Zolotarev (1996).

Sokolova *et al.* (1996) and Sherriff *et al.* (1998, 2000) stated that the *a* cell-dimension and ^{27}Al SATRAS NMR spectra show a continuous change across the series, which they interpreted as a continuous marialite–meionite solid-solution with three subseries characterized by different trends in atom substitutions and Si–Al order. However, the systematic behavior of the (CO_3) group across the series is not known, nor is its possible role in affecting the degree of Al–Si order across the series, particularly at short range. We will consider these issues, among others, in this and the following paper.

EXPERIMENTAL METHODS

The provenance of samples used in this work is shown in Table 2. The eighteen samples of scapolite cover most of the marialite–meionite solid-solution series, from $Me_{4.9}$ to $Me_{92.8}$ and from 3.10 to 5.62 Al *apfu*. These samples are primarily from granulite-facies metamorphic rocks and associated veins. Twelve of the eighteen samples have been studied previously by X-ray powder diffraction and NMR spectroscopy, and descriptions of samples S(1)–S(7), S(8), S(11), S(12), S(14) and S(16) can be found in Sokolova *et al.* (1996) and Sherriff *et al.* (1998, 2000). There are six new samples in this study, of which S(15) is of particular importance, as its composition corresponds closely to the change in symmetry from $I4/m$ to $P4_2/n$; it is a semitransparent yellowish scapolite from veins in metamorphic rocks of the Slyudyanka deposit, Russia. Sample S(8) is a gem-quality yellowish transparent scapolite from a Madagascar pegmatite. Samples S(10) and S(17) are yellowish transparent crystals from vugs

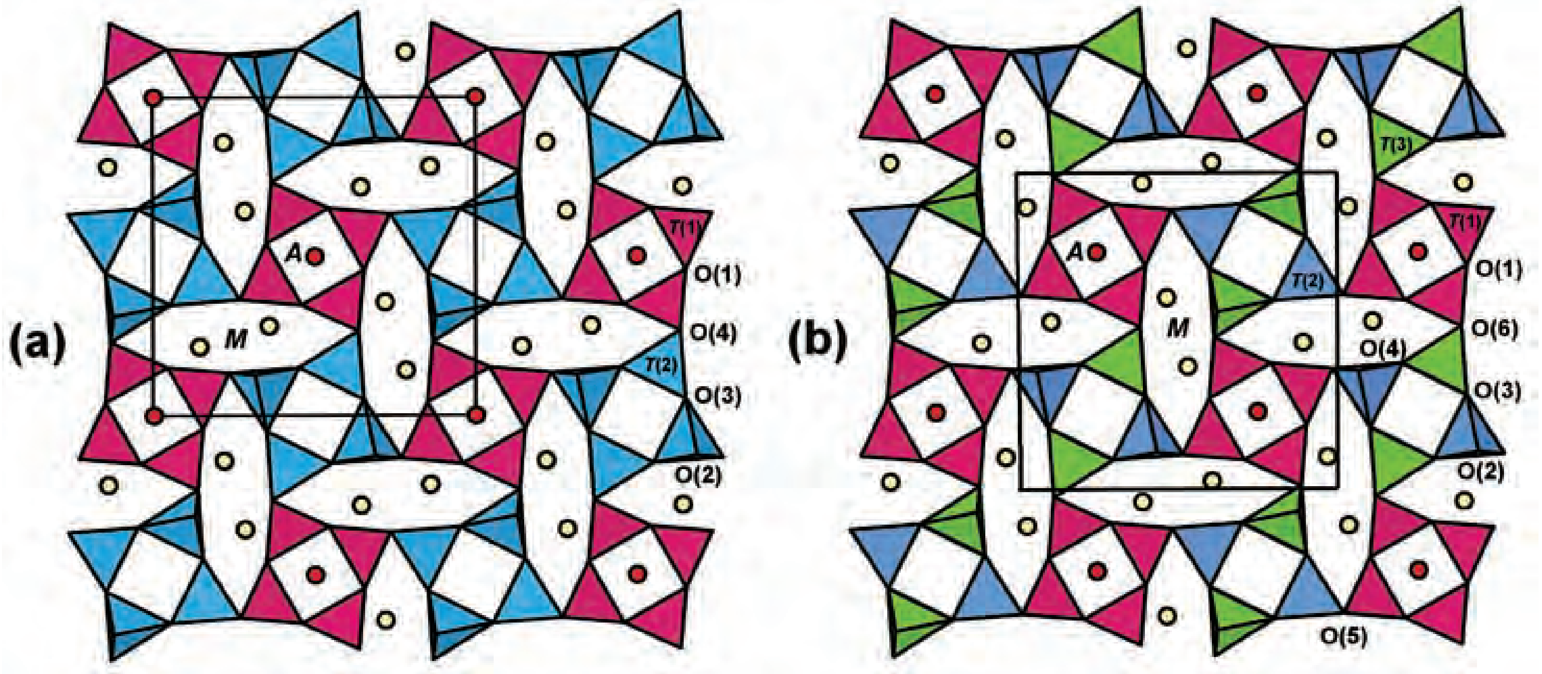

FIG. 1. The crystal structure of scapolite projected onto (001): (a) *I*4/*m*; (b) $P4_2/n$. The *T*(1) tetrahedra are pink, *T*(2) tetrahedra are blue, *T*(3) tetrahedra are green, Cl atoms are red circles, *M* atoms are yellow circles.

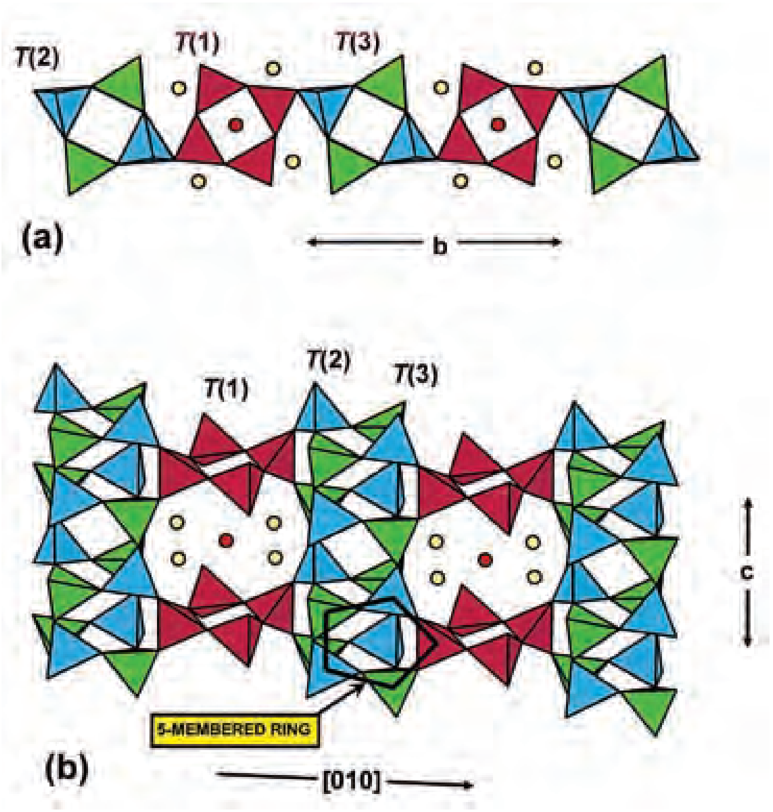

FIG. 2. A fragment of the crystal structure of scapolite: (a) viewed down [001]; (b) viewed down [100] ($P4_2/n$). Legend as in Figure 1.

TABLE 2. PROVENANCE OF SCAPOLITE CRYSTALS USED IN THIS WORK

No.	Sample code*	Me_x	Si *apfu*	Locality	Reference
S(1)	PAM-1	4.9	3.103	Pamir, Tajikistan	Sokolova *et al.* (1996)
S(2)	PAM-2	7.0	3.186	Pamir, Tajikistan	Sokolova *et al.* (1996)
S(3)	PAM-3	7.7	3.247	Pamir, Tajikistan	Sokolova *et al.* (1996)
S(4)	S-1	9.0	3.279	Pamir, Tajikistan	Sokolova *et al.* (2000)
S(5)	S-2	15.1	3.468	Pamir, Tajikistan	Sokolova *et al.* (2000)
S(6)	PAM-4	21.0	3.649	Pamir, Tajikistan	Sherriff *et al.* (1998)
S(7)	TANZ	26.4	3.745	Tanzania	Sherriff *et at.* (1998)
S(8)	–	28.7	3.801	Madagascar	This work
S(9)	PAM-5	32.3	3.873	Pamir, Tajikistan	Sherriff *et al.* (1998)
S(10)	–	42.0	4.102	Monte Somma, Italy	This work
S(11)	MAD	45.7	4.210	Madagascar	Sherriff *et al.* (1998)
S(12)	MIN	57.7	4.546	Minden, Canada	Sherriff *et al.* (1998)
S(13)	–	66.7	4.701	Pargas, Finland	This work
S(14)	BOLT	69.6	4.841	Bolton, USA	Sherriff *et al.* (2000)
S(15)	–	76.9	5.068	Sluydyanka, Russia	This work
S(16)	SL-1	78.4	5.147	Sluydyanka, Russia	Sherriff *et al.* (2000)
S(17)	–	88.1	5.445	Monte Somma, Italy	This work
S(18)	M–9122	92.8	5.617	Royal Ontario Museum	This work

* The code used for previous Rietveld structure refinement of powder X-ray data.

in marble blocks from Monte Somma, Italy; S(17) is slightly altered in the outer zones. Sample S(13) is an opaque yellowish white crystal from a metamorphic complex at Pargas, Finland. Sample S(18) is a gem-quality yellowish scapolite from Monte Somma, Italy. All samples were checked optically for homogeneity. We could not find inclusion-free crystals of samples S(2) and S(16), and were careful to avoid inclusions during electron-microprobe analysis.

Collection of X-ray data

Crystals used for the collection of single-crystal X-ray-diffraction data were selected on the basis of optical clarity, ground to spheres (or spheroids), and mounted on a Bruker *P*4 diffractometer fitted with a Smart 1K CCD detector and using Mo$K\alpha$ radiation. For each crystal, integrated intensities were collected for the whole sphere of reciprocal space using 30 s per frame. Unit-cell parameters were refined from approximately 4000 reflections with ($I > 10\ \sigma I$). An empirical absorption-correction (SADABS, Sheldrick 1998) was applied. Prior to data reduction, the intensity data were carefully checked for reflections violating the *I*-centered condition $h + k + l = 2n$. No violators were observed for samples S(1)–S(6) and S(16)–S(18), and the intensity data for S(1)–S(6) and S(16)–S(18) were processed in the space group *I*4/*m*. For samples S(7)–S(14), numerous observed reflections violate the condition $h + k + l = 2n$, and the intensity data were processed in the space group $P4_2/n$. For sample S(15), there are only two strong reflections violating the *I*-centered condition. The data were processed in both space groups, *I*4/*m* and $P4_2/n$. Details of data collection and refined unit-cell parameters are given in Table 3.

Electron-microprobe analysis

The chemical compositions of 18 single crystals used for collection of the X-ray intensity data were determined by electron-microprobe analysis (10 points per crystal) using a Cameca SX50 operating in wavelength-dispersion mode at 15 kV and 20 nA. The following standards were used: fluorine-bearing riebeckite (F), albite (Na), forsterite (Mg), scapolite (Si, Al), apatite (P), anhydrite (S), tugtupite (Cl), sanidine (K), anorthite (Ca), titanite (Ti), spessartine (Mn), fayalite (Fe), $SrTiO_3$ (Sr) and barite (Ba). Data were reduced using the "ZAF" correction (PUMA program). The unit formula (Table 4) of each crystal was calculated by normalizing to 12 *T* = (Si + Al) *apfu*. Thus we assume that there is no vacancy at the *T* site. The CO_2 content was calculated assuming that the *A* site is fully occupied by Cl, (SO_4) and (CO_3): (CO_3) = 1 – Cl – (SO_4); this assumption seems justified by the fact that the resulting amounts of species are in accord with the electron densities observed at and around the *A* site.

CRYSTAL-STRUCTURE REFINEMENT

The structures of 18 crystals were refined with the SHELXTL 5.1 software (Sheldrick 1997). Scattering factors for neutral metal atoms were taken from the International Tables for X-ray Crystallography (1992). Scattering curves for ionized species were used for O^{2-} and Cl^-. Crystals S(1)–S(6) and S(16)–S(18) were refined in space group *I*4/*m*; crystals S(7)–S(14) were refined in space group $P4_2/n$. The structure of S(15) was refined in both space groups, *I*4/*m* and $P4_2/n$. In the space group $P4_2/n$, the *T*(2) and *T*(3) tetrahedra are symmetrically distinct and hence are not required to have the same mean bond-lengths. In the space group *I*4/*m*, the *T*(2) and *T*(3) tetrahedra of the $P4_2/n$ structure are symmetrically equivalent and constitute the *T*(2) site. Thus we may test for the best space-group for S(15) by comparing the <*T*(2)–O> and <*T*(3)–O> bond lengths in the $P4_2/n$ refinement. If the distances are equal, the space group is I4/*m*; if the distances are not equal, then the space group is $P4_2/n$. The relevant distances are 1.691(2) and 1.666(2) Å, with a difference of 0.025(2) Å. This difference is significant at the 95% confidence limit, and hence we assign the space group $P4_2/n$ to crystal S(15).

Each structure was refined in two stages. At the primary stage of refinement, the *T* sites were assigned as Si, and their occupancies were fixed, the *A* site was assigned as Cl, and the occupancy was considered as variable; the structure was refined to convergence. At the secondary stage of the refinement, the site occupancies were adjusted by a combination of site-scattering refinement and assignment from the unit formula calculated from the chemical composition such that the site occupancies are equally in accord with the results of the site-scattering refinement and the unit formula.

Site scattering at the T sites

The occupancies of the *T* sites cannot be refined because of the very small difference in X-ray scattering between Si (*Z* = 14) and Al (*Z* = 13). On the basis of the EMPA data and the <*T*–O> bond-lengths derived from the primary refinement, Si and Al occupancies were assigned to each tetrahedral site (see later discussion) and fixed during subsequent stages of refinement.

Site scattering at the M site

The *M* site can be occupied by five cations, Na, Ca, Fe^{2+}, Sr and K, and we also cannot rule out the possibility of vacancies (□). For each crystal, the site occupancies of the dominant and minor cations were fixed at the values indicated by the unit formulae (Table 4), and the occupancy of the subordinate cation was refined. Thus for S(1), the site occupancies for Na (predominant), Fe^{2+}, Sr, and K were fixed at the

TABLE 3. MISCELLANEOUS REFINEMENT DATA FOR THE SCAPOLITE-GROUP MINERALS*

	S(1)	S(2)	S(3)	S(4)	S(5)	S(6)	S(7)	S(8)	S(9)
a (Å)	12.0570(5)	12.0541(5)	12.0566(5)	12.0538(5)	12.0471(5)	12.0450(5)	12.0720(5)	12.0753(4)	12.0793(5)
c (Å)	7.5644(3)	7.5682(3)	7.5696(3)	7.5714(3)	7.5793(3)	7.5826(3)	7.5854(3)	7.5864(3)	7.5842(3)
V (Å^3)	1099.7(1)	1099.7(1)	1100.3(1)	1100.1(1)	1100.0(1)	1100.1(1)	1105.4(1)	1106.2(1)	1106.6(1)
Z	2	2	2	2	2	2	2	2	2
Refl. I>10σI**	3958	4174	4100	3729	4272	4363	4078	5355	4522
Space group	*I4/m*	*I4/m*	*I4/m*	*I4/m*	*I4/m*	*I4/m*	$P4_2/n$	$P4_2/n$	$P4_2/n$
D_{calc} (g/cm^3)	2.584	2.589	2.594	2.591	2.591	2.616	2.632	2.640	2.654
Crystal size(mm)***	0.15 sphere	0.17 sphere	0.15 sphere	0.12 sphere	0.13×0.17 ×0.17	0.10×0.12 ×0.17	0.10×0.12 ×0.17	0.17 sphere	0.14×0.16 ×0.21
Abs.coef.(mm^{-1})	1.07	1.08	1.09	1.09	1.09	1.16	1.23	1.25	1.26
F(000)	944.9	946.9	948.8	947.8	947.8	957.5	968.1	972.0	978.2
2θ max (°)	60.01	60.00	60.01	60.02	59.96	59.96	59.98	59.96	59.94
R(int)	2.82	2.77	2.67	3.14	2.97	1.99	3.73	2.56	2.93
Refl. collected	6300	6304	6370	6300	6347	6357	12860	12833	12853
$F_o>4\sigma F$	5079	5070	5107	5077	5081	5122	10388	10319	10343
Unique reflections	854	853	857	854	848	853	1612	1609	1594
$F_o>4\sigma F$	767	776	772	750	767	768	1101	1269	1163
GooF on F^2	1.116	1.115	1.100	1.106	1.113	1.147	1.094	1.057	1.127
Final *R* indices									
$F_o>4\sigma F$	2.10	2.28	2.00	2.20	2.52	2.20	3.04	2.73	2.86
R indices (all data)									
R_1	2.44	2.56	2.33	2.67	2.82	2.50	4.53	3.47	3.98
wR_2	5.98	6.40	5.68	6.41	7.59	6.16	10.16	8.41	8.99
GooF	1.116	1.115	1.100	1.106	1.113	1.144	1.093	1.069	1.127

	S(10)	S(11)	S(12)	S(13)	S(14)	S(15)	S(16)	S(17)	S(18)
a (Å)	12.0915(5)	12.0972(5)	12.1338(5)	12.1498(6)	12.1520(5)	12.1674(5)	12.1713(5)	12.2050(4)	12.2077(5)
c (Å)	7.5841(3)	7.5814(3)	7.5755(3)	7.5681(4)	7.5673(3)	7.5779(3)	7.5801(3)	7.5816(3)	7.5832(3)
V (Å^3)	1108.8(1)	1109.5(1)	1115.3(1)	1117.2(2)	1117.5(1)	1121.9(1)	1122.9(1)	1129.38(4)	1130.1(1)
Z	2	2	2	2	2	2	2	2	2
Refl. I>10σI**	4285	4857	3995	3225	4330	4088	4232	4492	3867
Space group	$P4_2/n$	$P4_2/n$	$P4_2/n$	$P4_2/n$	$P4_2/n$	$P4_2/n$	*I4/m*	*I4/m*	*I4/m*
D_{calc} (g/cm^3)	2.678	2.675	2.708	2.700	2.703	2.760	2.759	2.724	2.749
Crystal size (mm)***	0.20 sphere	0.18 sphere	0.08×0.19 ×0.20	0.07×0.12 ×0.12	0.19 sphere	0.17 sphere	0.17 sphere	0.16 sphere	0.12×0.16 ×0.16
Abs.coef.(mm^{-1})	1.32	1.33	1.45	1.42	1.42	1.55	1.54	1.57	1.62
F(000)	989.9	989.6	1007.6	1007.5	1009.4	1034.2	1035.3	1026.9	1036.9
2θ max (°)	60.01	59.99	59.98	60.00	60.03	59.97	59.97	59.88	59.99
R(int)	3.44	3.10	3.11	3.96	2.61	2.85	2.62	2.78	2.76
Refl. collected									
$F_o>4\sigma F$	12926	12869	13032	12968	13056	13033	6479	6500	
	10380	10329	10488	10430	10471	10487	5212	5232	5211
Unique reflections	1613	1615	1622	1631	1631	1638	877	878	884
$F_o>4\sigma F$	1190	1248	1124	978	1136	854	789	815	786
GooF on F^2	0.979	1.105	0.939	0.923	0.993	1.070	0.021	1.066	1.044
Final *R* indices									
$F_o>4\sigma F$	2.68	2.59	2.58	2.73	2.31	2.47	2.17	2.42	2.33
R indices (all data)									
R_1	3.92	3.54	4.02	5.29	3.78	5.31	2.53	2.61	2.75
wR_2	7.73	8.29	7.42	7.24	6.95	8.26	5.65	6.24	5.90
GooF	0.983	1.123	0.945	0.956	0.998	1.070	1.029	1.077	1.060

* Radiation: Mo*K*α; refinement method: full-matrix least squares on F^2; fixed weights proportional to 1/s(F_o^2).

** Number of reflections for the determination of the final cell; *** diameter of a sphere.

TABLE 4. CHEMICAL COMPOSITION AND FORMULA UNIT OF SCAPOLITE-GROUP MINERALS

	S(1)	S(2)	S(3)	S(4)	S(5)	S(6)	S(7)	S(8)	S(9)	S(10)	S(11)	S(12)	S(13)	S(14)	S(15)	S(16)	S(17)	S(18)
SiO_2 wt.%	62.55	61.91	61.44	61.06	59.56	57.97	56.56	55.83	54.95	53.19	52.04	49.00	48.08	46.90	44.49	44.11	42.52	40.84
Al_2O_3	18.51	18.99	19.34	19.48	20.54	21.49	21.77	21.96	22.22	23.44	23.86	25.36	26.27	26.91	27.60	28.11	29.97	30.49
FeO	0.09	0.04	0.06	0.06	0.07	0.04	0.11	0.14	0.04	0.13	0.06	0.05	0.03	0.02	0.12	0.00	0.14	0.17
CaO	1.21	1.93	1.97	2.29	3.86	5.41	6.61	7.13	8.07	10.40	11.23	13.93	16.01	16.87	18.25	18.64	20.91	22.17
SrO	0.04	0.04	0.07	0.06	0.09	0.09	0.09	0.09	0.12	0.11	0.14	0.34	0.07	0.02	0.21	0.17	0.00	0.15
Na_2O	12.84	12.62	12.69	12.42	11.93	11.26	9.48	9.04	8.74	7.44	7.12	5.31	4.19	3.98	2.95	2.82	1.10	0.64
K_2O	1.58	1.27	1.41	1.24	0.59	0.26	1.39	1.47	1.13	0.92	0.50	0.66	0.37	0.14	0.18	0.08	0.72	0.48
SO_3	0.09	0.14	0.16	0.15	0.25	0.25	0.65	0.83	1.02	1.22	0.79	1.24	0.01	0.02	2.45	2.47	0.13	0.23
CO_2	0.05	0.19	0.18	0.24	0.42	0.65	0.84	0.90	1.30	1.89	2.22	2.78	4.05	4.18	3.26	3.40	4.30	4.41
Cl	4.07	3.97	3.93	3.87	3.67	3.46	3.08	2.93	2.49	1.91	1.80	1.09	0.62	0.49	0.08	0.11	0.28	0.12
O=Cl	–0.92	–0.90	–0.89	–0.87	–0.83	–0.78	–0.69	–0.66	–0.56	–0.43	–0.41	–0.25	–0.14	–0.11	–0.02	–0.02	–0.06	–0.03
Total	100.11	100.20	100.36	100.00	100.15	100.00	99.89	99.66	99.52	100.22	99.35	99.51	99.56	99.42	99.57	100.00	100.01	99.67
Si *apfu*	8.897	8.814	8.753	8.721	8.532	8.351	8.255	8.199	8.127	7.898	7.790	7.454	7.299	7.159	6.932	6.853	6.555	6.383
Al	3.103	3.186	3.247	3.279	3.468	3.649	3.745	3.801	3.873	4.102	4.210	4.546	4.701	4.841	5.068	5.147	5.445	5.617
Fe^{2+}	0.011	0.005	0.007	0.007	0.008	0.005	0.013	0.017	0.005	0.016	0.008	0.006	0.004	0.003	0.016	0.000	0.018	0.022
Ca	0.184	0.294	0.301	0.350	0.592	0.835	1.034	1.122	1.279	1.655	1.801	2.270	2.604	2.759	3.047	3.103	3.454	3.713
Sr	0.003	0.003	0.006	0.005	0.007	0.008	0.008	0.008	0.010	0.009	0.012	0.030	0.006	0.002	0.019	0.016	0.000	0.014
Na	3.541	3.483	3.505	3.439	3.314	3.145	2.683	2.574	2.506	2.142	2.067	1.566	1.233	1.178	0.891	0.849	0.329	0.194
K	0.287	0.231	0.256	0.226	0.108	0.048	0.259	0.275	0.213	0.174	0.095	0.128	0.072	0.027	0.036	0.016	0.142	0.096
ΣM	4.026	4.016	4.075	4.027	4.029	4.041	3.997	3.996	4.013	3.996	3.983	4.000	3.919	3.969	4.009	3.984	3.943	4.039
(SO_4)	0.010	0.015	0.017	0.016	0.027	0.027	0.071	0.091	0.113	0.136	0.089	0.142	0.001	0.002	0.286	0.288	0.015	0.027
(CO_3)	0.010	0.037	0.035	0.047	0.082	0.128	0.167	0.180	0.262	0.383	0.454	0.577	0.839	0.871	0.693	0.721	0.905	0.941
Cl	0.981	0.958	0.949	0.937	0.891	0.845	0.762	0.729	0.624	0.481	0.457	0.281	0.160	0.127	0.021	0.028	0.073	0.032
ΣA	1.001	1.010	1.001	1.000	1.000	1.000	1.000	1.000	0.999	1.000	1.000	1.000	1.000	1.000	1.000	1.037	0.993	1.000
O	24.118	24.206	24.218	24.229	24.384	24.534	24.820	24.942	25.270	25.721	25.742	26.319	26.519	26.631	27.246	27.304	26.803	27.064
% *Me*	4.9	7.0	7.7	9.0	15.1	21.0	26.4	28.7	32.3	42.0	45.7	57.7	66.7	69.6	76.9	78.4	88.1	92.8

Detection limits (wt.%): S 0.03–0.04, Mg 0.01, Sr 0.09, Fe 0.03, K 0.01, Mg not detected.

values indicated in Table 4, and the occupancy for Ca was refined.

Site-scattering refinement at the A site

The refined site-scattering at the *A* site invariably shows a good correlation with the unit formulae calculated from the chemical compositions (Table 4). Hence at the secondary stage of refinement, the site occupancies for Cl, C and S atoms were fixed at the values indicated by the unit formula: Cl + C + S = 1.0.

Refinement of the carbonate group

As noted above, the (CO_3) group must show some sort of long-range disorder where the *A* site is occupied by C. Similarly, the (SO_4) group may also show disorder for the same reason. The result is a complicated pattern of electron density around the *A* site (*e.g.*, Figs. 3, 4). Where there is no (SO_4) present in the unit cell, the electron density within ~2 Å of the *A* site is restricted to the (001) plane through the *A* site, indicating that the (CO_3) group is restricted to the (001) plane all across the series from marialite to meionite. In order to ensure consistency of the model used for the (CO_3) group across the series, difference-Fourier maps were calculated from the final structure-model with the oxyanion constituents of the *A* site removed from the model; selected maps are shown in Figure 3. There is no significant difference in the patterns of density in the $I4/m$ and $P4_2/n$ structures except for a slight difference in orientation (*cf.* Figs. 3g, h). As expected, the amount of residual density increases across the series, in parallel with the calculated (CO_3) content (Table 4). The pattern of density observed (Fig. 3) is similar to that observed in previous work, and thus we provisionally adopted the

FIG. 3. Difference-electron-density maps calculated omitting the (CO_3) group from the structure model: (a) S(6), (b) S(8), (c) S(9), (d) S(10), (e) S(11), (f) S(13), (g) S(15), (h) S(18). Contours are shown at intervals of 0.5 e/Å^3, negative contours are dashed, and the zero contour is omitted. Section z = 0.25 for (b)–(g) and z = 0.5 for (a) and (h). Length of the horizontal edge is 6 Å.

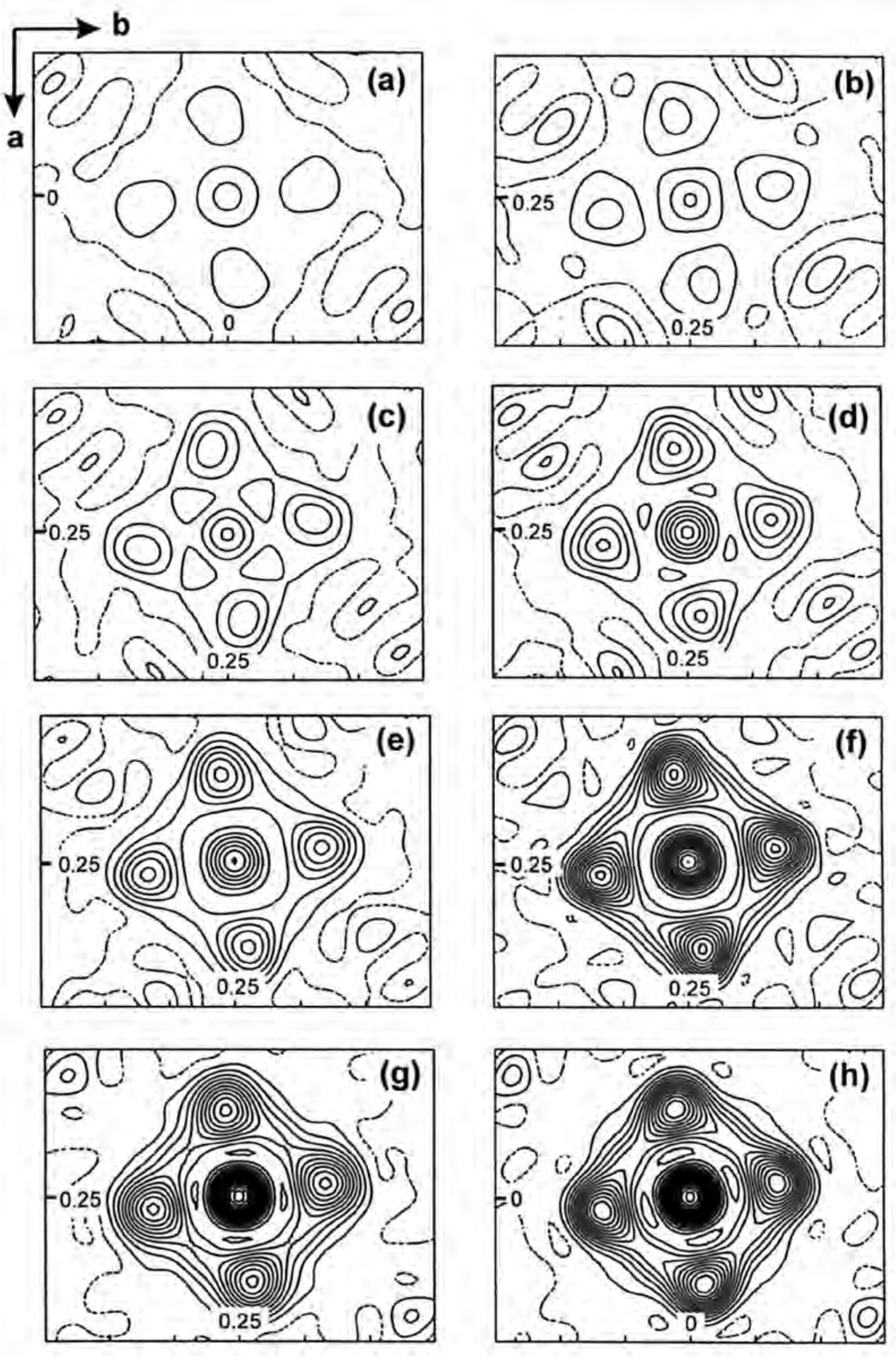
b
a
(a)
0
0
(b)
0.25
0.25
(c)
0.25
0.25
(d)
0.25
0.25
(e)
0.25
0.25
(f)
0.25
0.25
(g)
0.25
0.25
(h)
0
0

model of Levien & Papike (1976) as input to the refinement procedure. In Figure 3, the central density corresponds to four positions of the disordered C site, and the surrounding four maxima are the disordered O atoms of the (CO_3) group. The most intense set of maxima in these maps is that corresponding to the O(7) atom, and these maxima are detectable (≥ 1 e/Å^3) in scapolites S(6) [= 0.13 *apfu* (CO_3)] and S(7–18). Inclusion of the C and O(7) atoms into the difference-Fourier calculations allowed location of the two additional O atoms of the (CO_3) group (Fig. 4): they occur as "doublets" of density located ~1.3 Å from the central *A* site.

Where (CO_3) is the dominant component at the *A* site [*e.g.*, S(18)], refinement of the atoms of the (CO_3) group is fairly robust. However, as the meionite content

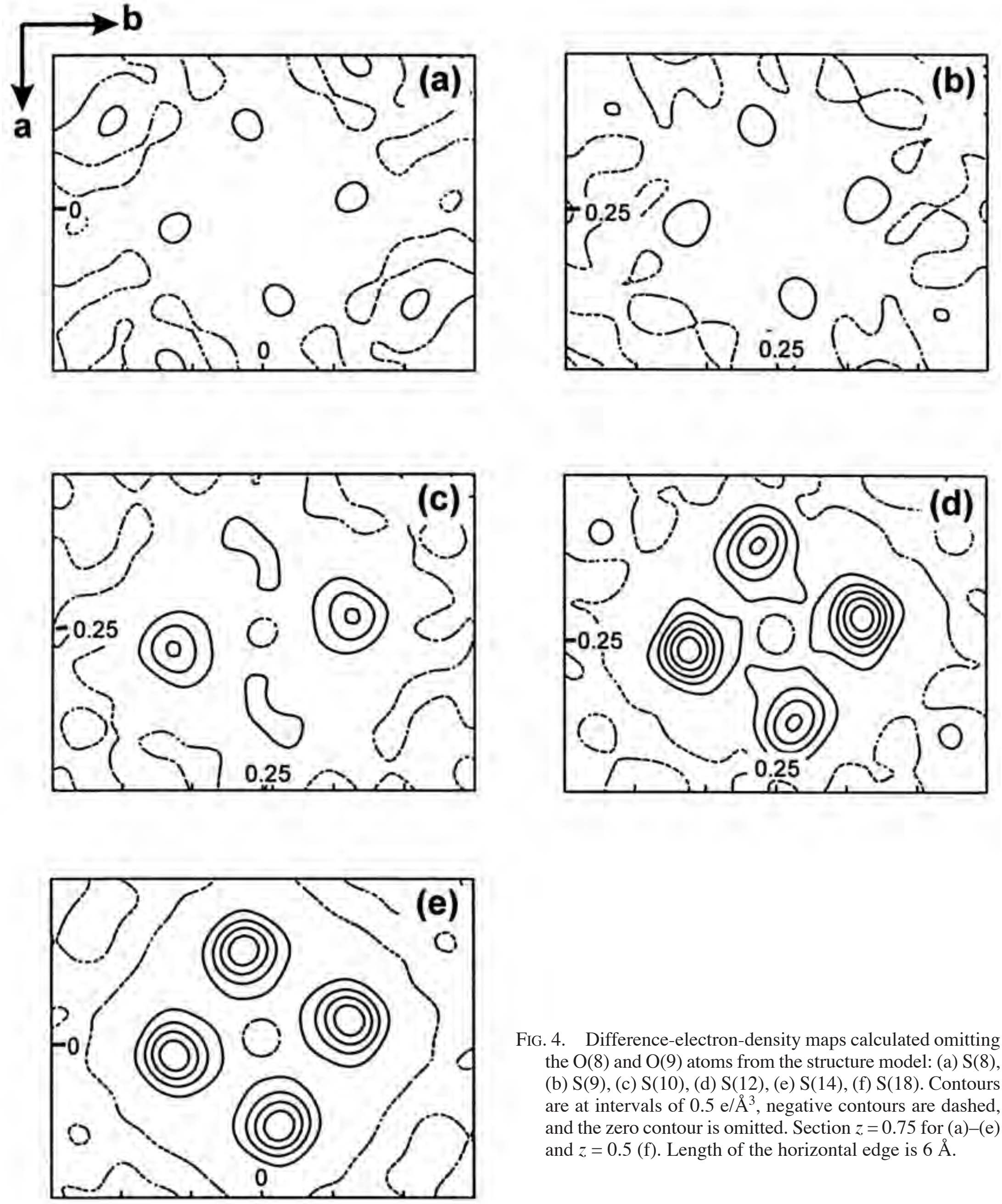

FIG. 4. Difference-electron-density maps calculated omitting the O(8) and O(9) atoms from the structure model: (a) S(8), (b) S(9), (c) S(10), (d) S(12), (e) S(14), (f) S(18). Contours are at intervals of 0.5 e/Å^3, negative contours are dashed, and the zero contour is omitted. Section $z = 0.75$ for (a)–(e) and $z = 0.5$ (f). Length of the horizontal edge is 6 Å.

of the crystals decreases, refinement becomes more difficult, and a more constrained model is required if we wish to gain detailed stereochemical information across the whole (or most of the) series. The refinement model used the following soft constraints: C–O(7) ≈ 1.32 Å, C–O(8) ≈ C–O(9) ≈1.26 Å [from observations on difference-Fourier maps for high-(CO_2) crystals]; O(7)–O(8) ≈ O(7)–O(9) ≈ O(8)–O(9) ≈ 2.30 Å. Moreover, the site occupancies of C, O(7), O(8) and O(9) were fixed at values derived in Table 4. Thus only positional and displacement parameters were refined, with the former softly constrained as indicated above. In this way, we were able to satisfactorily refine the (CO_3) group for crystals S(8) to S(18), *i.e.*, for crystals with ≥0.18 *apfu* (CO_3).

Refinement of the sulfate group

As noted by Peterson *et al*. (1979), the O atoms of the (SO_4) group have an expression as electron density close to the *A* site but both above and below the (001) plane through the *A* site. Figure 5 shows the residual density in this region of the structure, calculated in the same way as for the (CO_3) group. The intensity of this density scales well with the analyzed (SO_4) content of the crystals, and these atoms were detected for (SO_4) ≥ 0.27 *apfu*. Note that in *I*4/*m*, all O atoms of the (SO_4) group are symmetrically equivalent [= O(10); see below, Table 6], whereas in *P*4$_2$/*n*, there are two symmetrically distinct O atoms, O(10) and O(11) (see below, Table 7). The residual density forms eight equivalent maxima in *I*4/*m*, as required by symmetry, and this corresponds to (SO_4) groups in two distinct configurations related by a 90° rotation around the 4-fold rotation axis through the *A* site (Fig. 5e). In *P*4$_2$/*n*, the residual density forms two distinct sets [≡ O(10 and O(11)]. The densities at these two sites may be similar (*e.g*., Fig. 5d) or very different (*e.g*., Fig. 5c); the latter may denote anion ordering and will be discussed later.

As for the refinement of the (CO_3) group, constraints also were used for refinement of the (SO_4) group. The S–O(10) and S–O(11) distances were constrained to be equal to the values read from the difference-Fourier map, and the site occupancies were set such that the site populations of the S and O(10) sites were in accord with (SO_4) stoichiometry.

Details of the structure refinements are given in Table 3. Final atom-parameters and selected interatomic distances are given in Tables 5, 6 and Tables 7, 8, respectively. Atom-displacement parameters and structure factors may be obtained from The Depository of Unpublished Data on the MAC website [document Scapolite CM46_1527].

THE *T* SITES

Geometrical relations

Selected distances for *T*(1), *T*(2) and *T*(3) sites are given in Tables 7 (*I*4/*m*) and 8 (*P*4$_2$/*n*). The grand <*T*–O> distance is a linear function of Al content in *apfu* (Fig. 6a), and linear regression gives the following relation:

$$\langle T\text{–O}\rangle = 1.6027(6) + 0.0127(1)\ \text{Al}\ (apfu) \quad R^2 = 0.998 \qquad (1)$$

Division of the trend into three parts, corresponding to the different space-group symmetries, gives the following trends for <*T*–O> as a function of Al content (*apfu*):

$$\text{S(1)–S(6)} \quad I4/m \quad \langle T\text{–O}\rangle = 1.594(7) + 0.015(2)\ \text{Al} \quad R^2 = 0.928 \qquad (2)$$

$$\text{S(7)–S(15)} \quad P4_2/n \quad \langle T\text{–O}\rangle = 1.6069(7) + 0.0118(2)\ \text{Al} \quad R^2 = 0.999 \qquad (3)$$

$$\text{S(16)–S(18)} \quad I4/m \quad \langle T\text{–O}\rangle = 1.598(8) + 0.014(1)\ \text{Al} \quad R^2 = 0.989 \qquad (4)$$

The regression lines for S(1)–S(6) and S(16)–S(18) are not significantly different, and hence we can fit the two sets of *I*4/*m* data to a single curve:

$$\langle T\text{–O}\rangle = 1.6019(5) + 0.0129(1)\ \text{Al} \quad R^2 = 0.999 \qquad (5)$$

The differences between the intercepts and slopes of equations (3) and (5), together with the associated pooled standard deviations, are as follows: 0.0050(8) and 0.0011(2), respectively. For equations (3) and (5) to be significantly different, the values given above must be significantly different from zero; as the differences are all ~6σ, equations (3) and (5) are significantly different. Figure 6b shows all the data for crystals S(1)–S(18) with the regression line calculated only for crystals S(7)–S(15) [*i.e*., equation (3)]; it is apparent from Figure 6b that there are subtle differences between the structural responses of the *I*4/*m* and *P*4$_2$/*n* structures to variations in Al content.

The T(1) site

There are three trends in <*T*(1)–O> distances as a function of the content of Al (*apfu*) (Fig. 7a):

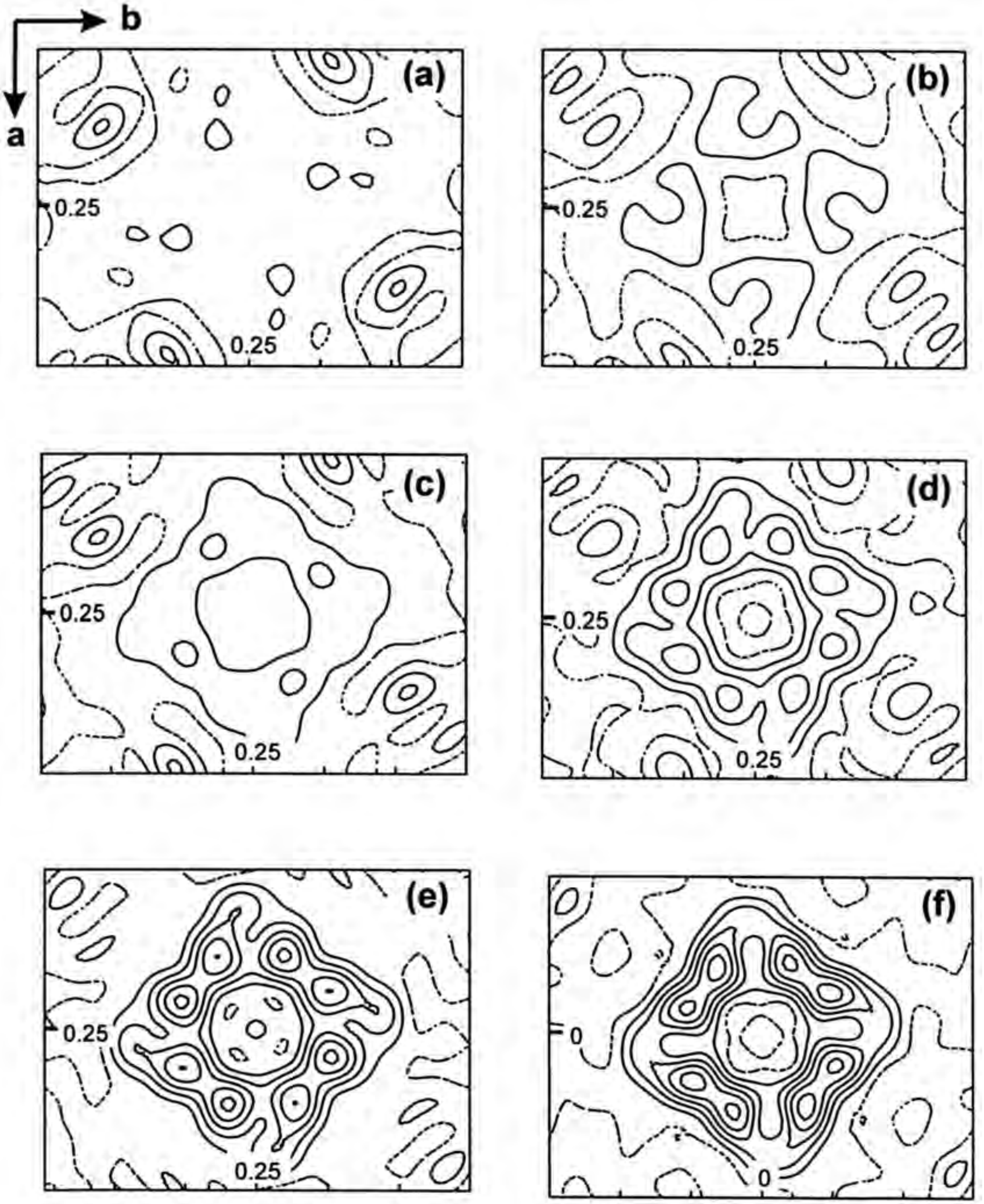

FIG. 5. Difference-electron-density maps calculated omitting the O(10) and O(11) atoms from the structure model: (a) S(6), 0.027 (SO_4); (b) S(8), 0.091 (SO_4); (c) S(10), 0.113 (SO_4); (d) S(15), 0.286 (SO_4); (e) S(16), 0.288 (SO_4) *pfu*. Contours are shown at intervals of 0.5 e/Å^3, negative contours are dashed, and the zero contour is omitted. Section $z = 0.6$ for (a)–(d) and $z = 0.85$ for (b) and (c). Length of the horizontal edge is 6 Å.

S(1)–S(6) $I4/m$ $\langle T(1)\text{–O}\rangle = 1.601(3) + 0.0018(8)\ \text{Al}$ $R^2 = 0.559$ (6)

S(7)–S(15) $P4_2/n$ $\langle T(1)\text{–O}\rangle = 1.493(5) + 0.030(1)\ \text{Al}$ $R^2 = 0.991$ (7)

S(16)–S(18) $I4/m$ $\langle T(1)\text{–O}\rangle = 1.599(9) + 0.0134(16)\ \text{Al}$ $R^2 = 0.986$ (8)

For crystals S(1)–S(6), which have space-group symmetry $I4/m$, the grand <*T*(1)–O> distance is 1.6066(5) Å, and there is no significant change in <*T*(1)–O> as a function of Al content. Thus there is a major discontinuity between $I4/m$ marialite and $P4_2/n$ scapolite (Fig. 7a). Moreover, we may conclude either that (1) the *T*(1) tetrahedron is fully occupied by Si, or that (2) there are small amounts of Al at *T*(1), but these crystals do not follow a hard-sphere model, or (3) $^{T(1)}$Al is approximately constant and non-zero from S(1) to S(6). For crystals S(7)–S(15), which have space-group symmetry $P4_2/n$, <*T*(1)–O> is a linear function of Al content, indicating that Al substitutes for Si at the *T*(1) site. The <*T*(1)–O> values for S(7) and S(8) are 1.607 and 1.608 Å, respectively. Do these two crystals contain Al at the *T*(1) site? Figure 7a suggests that S(8) does have Al at *T*(1), but the situation for S(7) is somewhat ambiguous. However, S(7) definitely has space-group symmetry $P4_2/n$, and the Occam's razor solution is

TABLE 5. FINAL ATOM PARAMETERS FOR THE SCAPOLITE-GROUP MINERALS IN $I4/m$

		S(1)	S(2)	S(3)	S(4)	S(5)	S(6)	S(16)	S(17)	S(18)
T(1)	*x*	0.16184(4)	0.16174(4)	0.16173(4)	0.16166(4)	0.16136(4)	0.16118(4)	0.16074(4)	0.16063(5)	0.16045(4)
	y	0.08892(4)	0.08930(4)	0.08929(4)	0.08946(4)	0.09020(4)	0.09067(4)	0.09196(4)	0.09218(5)	0.09249(1)
	z	0	0	0	0	0	0	0	0	0
	U_{eq}	0.0097(1)	0.0094(1)	0.0094(1)	0.0096(1)	0.0092(2)	0.0091(1)	0.0094(1)	0.0103(2)	0.0101(2)
T(2)	*x*	0.16232(3)	0.16238(3)	0.16242(3)	0.16243(3)	0.16253(3)	0.16255(3)	0.16017(3)	0.15994(4)	0.15994(3)
	y	0.41546(3)	0.41521(3)	0.41527(3)	0.41517(3)	0.41466(3)	0.41434(3)	0.41304(3)	0.41322(4)	0.41307(3)
	z	0.20677(4)	0.20670(5)	0.20671(5)	0.20670(5)	0.20665(5)	0.2066(1)	0.20691(5)	0.20703(6)	0.20705(5)
	U_{eq}	0.0101(1)	0.0099(1)	0.0100(1)	0.0101(1)	0.0099(2)	0.0100(1)	0.0107(1)	0.0111(2)	0.0109(1)
M	*x*	0.37137(8)	0.37024(9)	0.37031(8)	0.36984(9)	0.36755(9)	0.36609(8)	0.35772(4)	0.35665(5)	0.35652(4)
	y	0.29414(8)	0.29295(9)	0.29285(8)	0.29218(9)	0.28966(9)	0.28795(8)	0.28246(4)	0.28132(5)	0.28101(4)
	z	0	0	0	0	0	0	0	0	0
	U_{eq}	0.0435(4)	0.0425(4)	0.0421(4)	0.0412(4)	0.0372(4)	0.0345(4)	0.0248(2)	0.0263(2)	0.0256(2)
O(1)	*x*	0.0434(1)	0.0431(1)	0.0432(1)	0.0429(1)	0.0423(1)	0.0419(1)	0.0415(1)	0.0414(2)	0.0413(1)
	y	0.1485(1)	0.1487(1)	0.1486(1)	0.1486(1)	0.1489(1)	0.1488(1)	0.1517(1)	0.1523(2)	0.1526(1)
	z	0	0	0	0	0	0	0	0	0
	U_{eq}	0.0174(3)	0.0173(3)	0.0174(3)	0.0172(3)	0.0163(3)	0.0163(3)	0.0179(3)	0.0201(4)	0.0197(3)
O(2)	*x*	0.1938(1)	0.1938(1)	0.1940(1)	0.1941(1)	0.1942(1)	0.1942(1)	0.1866(1)	0.1868(2)	0.1868(1)
	y	0.3815(1)	0.3810(1)	0.3812(1)	0.3810(1)	0.3799(1)	0.3788(1)	0.3725(1)	0.3730(1)	0.3728(1)
	z	0	0	0	0	0	0	0	0	0
	U_{eq}	0.0179(3)	0.0177(3)	0.0174(3)	0.0175(3)	0.0175(3)	0.0178(3)	0.0164(3)	0.0179(4)	0.0172(3)
O(3)	*x*	0.44780(8)	0.44778(9)	0.44773(9)	0.44767(9)	0.4477(1)	0.4478(1)	0.44944(9)	0.4495(1)	0.44950(9)
	y	0.15019(8)	0.15030(9)	0.15033(9)	0.15050(9)	0.1511(1)	0.1514(1)	0.15064(9)	0.1506(1)	0.15068(9)
	z	0.2164(1)	0.2160(1)	0.2161(1)	0.2158(1)	0.2152(2)	0.2143(2)	0.2065(1)	0.2059(2)	0.2058(2)
	U_{eq}	0.0210(2)	0.0209(3)	0.0209(2)	0.0205(3)	0.0202(3)	0.0201(3)	0.0192(2)	0.0202(3)	0.0192(3)
O(4)	*x*	0.27067(8)	0.27067(9)	0.27075(9)	0.27080(9)	0.2710(1)	0.2712(1)	0.26683(9)	0.2663(1)	0.26621(9)
	y	0.37263(8)	0.37220(9)	0.37224(8)	0.37199(9)	0.3709(1)	0.3702(1)	0.36535(9)	0.3646(1)	0.36400(9)
	z	0.6732(1)	0.6732(1)	0.6732(1)	0.6731(1)	0.6729(2)	0.6729(2)	0.6733(2)	0.6742(2)	0.6741(2)
	U_{eq}	0.0202(2)	0.0202(3)	0.0200(2)	0.0198(3)	0.0196(3)	0.0188(3)	0.0223(3)	0.0225(3)	0.0224(3)
A	*x*	0	0	0	0	0	0	0	0	0
	y	0	0	0	0	0	0	0	0	0
	z	½	½	½	½	½	½	½	½	½
	U_{eq}	0.0522(4)	0.0510(4)	0.0513(4)	0.0507(4)	0.0502(5)	0.0502(5)	0.0147(17)	0.15(13)	0.10(6)
*C**	*x*	–	–	–	–	–	–	0.009(3)	0.015(3)	0.010(2)
	y	–	–	–	–	–	–	–0.014(2)	0.002(3)	0.000(4)
	z	–	–	–	–	–	–	½	½	½
	U_{eq}	–	–	–	–	–	–	0.062(8)	0.04(3)	0.032(11)

TABLE 5 (cont'd). FINAL ATOM PARAMETERS FOR THE SCAPOLITE-GROUP MINERALS IN *I*4/*m*

		S(1)	S(2)	S(3)	S(4)	S(5)	S(6)	S(16)	S(17)	S(18)
O(7)	*x*	–	–	–	–	–	0.107(2)	0.112(2)	0.122(2)	0.117(2)
	y	–	–	–	–	–	0.023(6)	0.019(2)	0.018(3)	0.018(3)
	z	–	–	–	–	–	½	½	½	½
	U_{eq}	–	–	–	–	–	0.018(19)	0.027(4)	0.028(4)	0.020(3)
O(8)	*x*	–	–	–	–	–	0.019(6)	–0.068(4)	–0.043(4)	–0.047(7)
	y	–	–	–	–	–	0.093(2)	0.056(5)	0.088(5)	0.086(8)
	z	–	–	–	–	–	½	½	½	½
	U_{eq}	–	–	–	–	–	0.03(2)	0.13(2)	0.053(9)	0.054(12)
O(9)	*x*	–	–	–	–	–	–	–0.005(3)	–0.018(5)	–0.021(7)
	y	–	–	–	–	–	–	–0.118(3)	–0.096(4)	–0.098(6)
	z	–	–	–	–	–	–	½	½	½
	U_{eq}	–	–	–	–	–	–	0.25(4)	0.047(8)	0.047(11)
O(10)	*x*	–	–	–	–	–	0.015(8)	0.021(1)	–	–
	y	–	–	–	–	–	–0.102(4)	–0.0973(9)	–	–
	z	–	–	–	–	–	0.59(2)	0.594(2)	–	–
	U_{eq}	–	–	–	–	–	0.009(23)	0.036(3)	–	–

**C* shifted from the *A* site.

that Al increases at *T*(1) in the $P4_2/n$ structure at all Si values. Thus Al occupies the *T*(1) site at ~3.7 Al *apfu* (~Me_{24}). This is not in accord with the prediction of Hassan & Buseck (1988) that Al begins to occupy the *T*(1) site at a Si:Al ratio of 2:1, *i.e.*, 4.0 Al *apfu* and $Me_{37.5}$. The trends of Figure 7a show that their proposal cannot be correct. At Al = 4.0 *apfu*, <*T*(1)–O> is equal to 1.6130 Å, whereas for S(1–6), <<*T*(1)–O>> is equal to 1.6066(5) Å. The difference between these values is 0.0064 Å with a pooled standard deviation of 0.0013 Å. This difference amounts to 4.9 σ and is significant; Al does *not* begin to occupy the *T*(1) site at Al = 4.0 *apfu* (*i.e.*, $Me_{37.5}$).

For crystals S(16)–S(18), <*T*(1)–O> is a single linear function of the total Al content; simple tests of the hypothesis show that the regression equations (7) and (8) above are significantly different. Thus there is a discontinuity where the space group changes from $P4_2/n$ to $I4/m$ for meionite.

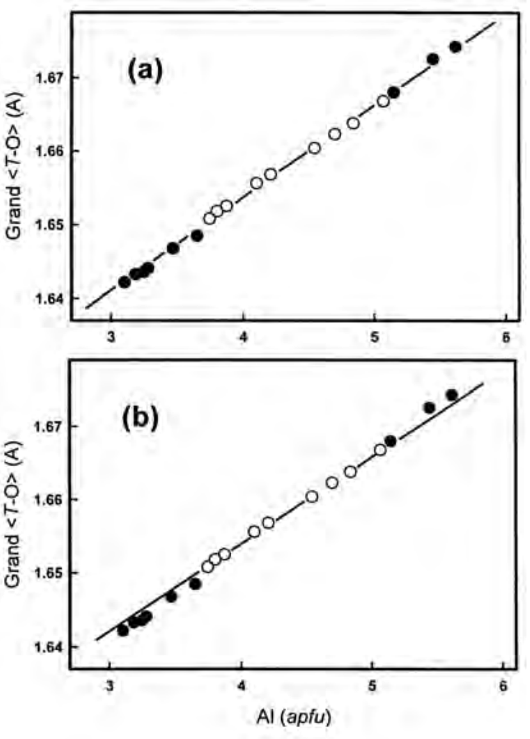

FIG. 6. Variation in grand <*T*–O> distance in the crystal structure of scapolite with Al *apfu*: (a) fitted to a single linear trend for S(1)–S(18); (b) fitted to a single trend for S(7)–S(15) only. Black circles are *I*4/*m* structures, white circles are $P4_2/n$ structures.

The T(2) and T(3) sites

At the $I4/m \rightarrow P4_2/n$ transition, the *T*(2) site splits into two sites, *T*(2) and *T*(3) (Table 1). The variation in aggregate <*T*–O> distances is shown in Figure 7b. Three distinct linear trends can be recognized as a function of content of Al (*apfu*):

$$\text{S(1)–S(6)} \quad I4/m \quad \langle T(2)\text{–O}\rangle = 1.6076(14) + 0.0169(4)\,\text{Al} \qquad R^2 = 0.997 \qquad (9)$$

$$\text{S(7)–S(15)} \quad P4_2/n \quad \langle T(2,3)\text{–O}\rangle = 1.662(3) + 0.0032(7)\,\text{Al} \qquad R^2 = 0.723 \qquad (10)$$

TABLE 6. FINAL ATOM PARAMETERS FOR THE SCAPOLITE-GROUP MINERALS IN $P4_2/n$

		S(7)	S(8)	S(9)	S(10)	S(11)	S(12)	S(13)	S(14)	S(15)
T(1)	x	0.58886(4)	0.58894(3)	0.58893(4)	0.58912(4)	0.58913(4)	0.58909(3)	0.58899(4)	0.58906(3)	0.58924(3)
	y	0.65980(4)	0.65975(4)	0.65954(4)	0.65920(4)	0.65902(4)	0.65902(4)	0.65878(4)	0.65851(3)	0.65822(4)
	z	0.74756(7)	0.74730(5)	0.74760(5)	0.74736(5)	0.74730(5)	0.74783(6)	0.74772(9)	0.74758(6)	0.7495(1)
	U_{eq}	0.0081(2)	0.0085(1)	0.0081(2)	0.0082(1)	0.0087(1)	0.0085(1)	0.0084(1)	0.0092(1)	0.0096(1)
T(2)	x	0.91042(5)	0.91015(4)	0.91002(4)	0.90915(4)	0.90902(4)	0.90845(4)	0.90836(5)	0.90815(4)	0.90941(7)
	y	0.16594(5)	0.16606(4)	0.16575(4)	0.16586(4)	0.16563(4)	0.16537(4)	0.16488(5)	0.16476(4)	0.16380(7)
	z	0.54770(7)	0.54828(6)	0.54782(6)	0.54861(6)	0.54852(6)	0.54745(6)	0.54712(8)	0.54733(6)	0.5439(1)
	U_{eq}	0.0090(2)	0.0093(1)	0.0090(2)	0.0095(1)	0.0100(2)	0.0101(1)	0.0095(2)	0.0101(1)	0.0111(2)
T(3)	x	0.66347(4)	0.66330(3)	0.66315(4)	0.66245(4)	0.66236(4)	0.66233(4)	0.66224(5)	0.66203(3)	0.66248(7)
	y	0.08589(4)	0.08574(3)	0.08604(4)	0.08586(4)	0.08608(4)	0.08700(4)	0.08783(5)	0.08781(3)	0.08902(7)
	z	0.46056(7)	0.46107(5)	0.46062(5)	0.46135(5)	0.46128(5)	0.46064(5)	0.46032(7)	0.46049(5)	0.4578(1)
	U_{eq}	0.0086(2)	0.0091(1)	0.0088(2)	0.0085(1)	0.0090(1)	0.0089(1)	0.0087(2)	0.0096(1)	0.0101(2)
M	x	0.11562(7)	0.11510(6)	0.11425(6)	0.11230(5)	0.11124(5)	0.10963(4)	0.10836(4)	0.10784(3)	0.10789(4)
	y	0.03767(6)	0.03730(6)	0.03687(6)	0.03559(5)	0.03497(5)	0.03431(4)	0.03385(4)	0.03334(3)	0.03277(4)
	z	0.7388(1)	0.73735(8)	0.73840(7)	0.73645(7)	0.73659(7)	0.73831(6)	0.74017(8)	0.73943(6)	0.7473(1)
	U_{eq}	0.0329(3)	0.0311(3)	0.0299(3)	0.0271(2)	0.0261(2)	0.0261(2)	0.0250(2)	0.0246(2)	0.0251(2)
O(1)	x	0.7080(1)	0.7080(1)	0.7083(1)	0.7084(1)	0.7086(1)	0.7084(1)	0.7084(1)	0.70846(9)	0.7085(1)
	y	0.6016(1)	0.6016(1)	0.6013(1)	0.6012(1)	0.6008(1)	0.6000(1)	0.5995(1)	0.59920(9)	0.5987(1)
	z	0.7521(2)	0.7523(2)	0.7521(2)	0.7522(2)	0.7523(1)	0.7517(1)	0.7519(1)	0.7516(1)	0.7504(3)
	U_{eq}	0.0143(3)	0.0147(3)	0.0141(3)	0.0144(3)	0.0154(3)	0.0156(3)	0.0158(3)	0.0170(2)	0.0173(3)
O(2)	x	0.9433(1)	0.9433(1)	0.9422(1)	0.9412(1)	0.9407(1)	0.9383(1)	0.9369(1)	0.9367(1)	0.9365(1)
	y	0.1286(1)	0.1280(1)	0.1269(1)	0.1255(1)	0.1249(1)	0.1238(1)	0.1228(1)	0.12243(9)	0.1227(1)
	z	0.7597(2)	0.7610(1)	0.7602(1)	0.7622(1)	0.7619(1)	0.7604(1)	0.7589(2)	0.7594(1)	0.7525(3)
	U_{eq}	0.0159(3)	0.0157(3)	0.0154(3)	0.0147(3)	0.0158(3)	0.0154(3)	0.0149(3)	0.0155(2)	0.0165(3)
O(3)	x	0.5999(1)	0.6000(1)	0.6002(1)	0.6004(1)	0.6006(1)	0.6011(1)	0.6013(1)	0.60141(9)	0.5998(2)
	y	0.1921(1)	0.1915(1)	0.1921(1)	0.1910(1)	0.1913(1)	0.1924(1)	0.1943(1)	0.19377(9)	0.1979(2)
	z	0.5412(2)	0.5422(2)	0.5428(2)	0.5454(2)	0.5460(1)	0.5466(1)	0.5471(2)	0.5480(2)	0.5448(3)
	U_{eq}	0.0184(4)	0.0184(3)	0.0175(3)	0.0166(3)	0.0171(3)	0.0172(3)	0.0177(4)	0.0177(3)	0.0196(5)
O(4)	x	0.7971(1)	0.7963(1)	0.7963(1)	0.7947(1)	0.7948(1)	0.79478(9)	0.7957(1)	0.79521(9)	0.7989(2)
	y	0.0975(1)	0.0972(1)	0.0972(1)	0.0968(1)	0.0969(1)	0.0975(1)	0.0982(1)	0.09788(9)	0.0992(2)
	z	0.4681(2)	0.4685(2)	0.4671(2)	0.4666(2)	0.4658(1)	0.4635(1)	0.4615(2)	0.4613(1)	0.4579(3)
	U_{eq}	0.0183(3)	0.0184(3)	0.0173(3)	0.0166(3)	0.0163(3)	0.0166(3)	0.0168(4)	0.0168(3)	0.0193(5)
O(5)	x	0.6193(1)	0.6190(1)	0.6187(1)	0.6177(1)	0.6174(1)	0.6165(1)	0.6163(1)	0.61553(9)	0.6153(2)
	y	0.9794(1)	0.9795(1)	0.9799(1)	0.9806(1)	0.9807(1)	0.9824(1)	0.9825(1)	0.98283(9)	0.9838(2)
	z	0.9218(2)	0.9218(2)	0.9213(2)	0.9207(2)	0.9213(2)	0.9212(2)	0.9234(2)	0.9234(2)	0.9225(3)
	U_{eq}	0.0179(4)	0.0182(3)	0.0174(3)	0.0180(3)	0.0184(3)	0.0191(3)	0.0185(4)	0.0195(3)	0.0220(6)
O(6)	x	0.5215(1)	0.5216(1)	0.5216(1)	0.5216(1)	0.5211(1)	0.5198(1)	0.5188(1)	0.51849(9)	0.5178(2)
	y	0.6218(1)	0.6218(1)	0.6216(1)	0.6213(1)	0.6207(1)	0.6197(1)	0.6187(1)	0.61811(9)	0.6160(2)
	z	0.9220(2)	0.9224(2)	0.9227(2)	0.9238(2)	0.9237(2)	0.9249(2)	0.9242(2)	0.9244(2)	0.9239(3)
	U_{eq}	0.0167(3)	0.0170(3)	0.0163(3)	0.0163(3)	0.0170(3)	0.0179(3)	0.0182(4)	0.0185(3)	0.0221(6)
A	x	¼	¼	¼	¼	¼	¼	¼	¼	¼
	y	¼	¼	¼	¼	¼	¼	¼	¼	¼
	z	¾	¾	¾	¾	¾	¾	¾	¾	¾
	U_{eq}	0.0550(5)	0.0547(9)	0.0471(10)	0.0392(13)	0.0417(16)	0.0307(12)	0.1194(159)	0.0333(8)	0.018(4)
C^*	x	–	0.283(7)	0.267(4)	0.261(3)	0.258(3)	0.266(2)	0.262(3)	0.258(3)	0.268(3)
	y	–	0.265(5)	0.252(4)	0.250(4)	0.252(3)	0.248(3)	0.249(2)	0.258(2)	0.250(3)
	z	–	0.75(1)	0.744(7)	0.71(1)	0.742(6)	0.726(5)	0.724(7)	0.750(7)	0.753(8)
	U_{eq}	–	0.14(9)	0.31(12)	0.12(3)	0.16(4)	0.14(3)	0.013(7)	0.073(9)	0.034(9)

TABLE 6 (cont'd). FINAL ATOM PARAMETERS FOR THE SCAPOLITE-GROUP MINERALS IN $P4_2/n$

		S(7)	S(8)	S(9)	S(10)	S(11)	S(12)	S(13)	S(14)	S(15)
O(7)	*x*	0.356(1)	0.393(7)	0.374(3)	0.366(3)	0.368(1)	0.370(1)	0.369(1)	0.364(1)	0.374(2)
	y	0.265(5)	0.258(7)	0.261(5)	0.262(3)	0.262(2)	0.273(2)	0.268(2)	0.252(2)	0.267(2)
	z	0.742(5)	0.73(2)	0.73(1)	0.749(3)	0.748(3)	0.738(3)	0.747(5)	0.745(4)	0.738(9)
	U_{eq}	0.036(16)	0.5(3)	0.025(10)	0.018(6)	0.018(4)	0.011(3)	0.020(3)	0.028(4)	0.046(10)
O(8)	*x*	–	0.233(7)	0.210(6)	0.214(3)	0.209(2)	0.194(3)	0.203(3)	0.217(1)	0.208(4)
	y	–	0.364(5)	0.343(8)	0.347(5)	0.350(2)	0.325(4)	0.338(3)	0.355(2)	0.338(4)
	z	–	0.76(1)	0.75(1)	0.715(8)	0.730(5)	0.735(5)	0.745(5)	0.749(4)	0.744(3)
	U_{eq}	–	0.02(1)	0.06(1	0.073(18)	0.054(9)	0.129(15)	0.058(11)	0.025(3)	0.065(13)
O(9)	*x*	–	0.22(1)	0.222(9)	0.212(8)	0.208(3)	0.239(3)	0.230(3)	0.201(4)	0.234(3)
	y	–	0.172(5)	0.158(5)	0.162(7)	0.158(4)	0.147(2)	0.149(2)	0.168(4)	0.152(3)
	z	–	0.75(2)	0.76(1)	0.750(7)	0.760(4)	0.744(3)	0.756(5)	0.753(3)	0.742(5)
	U_{eq}	–	0.09(5)	0.074(19)	0.10(2)	0.15(4)	0.038(6)	0.051(6)	0.108(12)	0.050(8)
O(10)	*x*	0.358(2)	0.357(2)	0.357(2)	–	–	–	–	–	0.349(2)
	y	0.272(5)	0.271(4)	0.268(5)	–	–	–	–	–	0.271(2)
	z	0.805(6)	0.822(8)	0.820(6)	–	–	–	–	–	0.847(3)
	U_{eq}	0.000(14)	0.028(11)	0.036(11)	–	–	–	–	–	0.041(7)
O(11)	*x*	0.355(2)	0.352(2)	0.348(2)	0.353(1)	0.353(2)	0.351(1)	–	–	0.344(1)
	y	0.267(4)	0.270(3)	0.265(3)	0.266(2)	0.265(2)	0.267(2)	–	–	0.264(2)
	z	0.669(5)	0.657(5)	0.648(3)	0.665(3)	0.662(3)	0.658(2)	–	–	0.640(3)
	U_{eq}	0.008(10)	0.026(8)	0.013(6)	0.043(4)	0.033(5)	0.045(5)	–	–	0.031(7)

**C* shifted from the *A* site.

S(16)–S(18) *I*4/*m* $\langle T(2)\text{–O}\rangle = 1.6410(2) + 0.0074(1)\ \text{Al}$ $R^2 = 0.999$ (11)

where $\langle T(2,3)\text{–O}\rangle = [\langle T(2)\text{–O}\rangle + \langle T(3)\text{–O}\rangle] / 2$. Linear trends (9) and (11) indicate that Al is more strongly ordered at the *T*(2) site in *I*-centered marialite than in *I*-centered meionite. Moreover, comparison of equations (7) and (10) is quite instructive. The slope of equation (7) is ten times that of equation (10), indicating that Al is ordering at *T*(1) much more rapidly than at *T*(2,3) with increasing Al content in the $P4_2/n$ structure; note that this observation is also in accord with the values for the intercepts in equations (7) and (10).

The variation in <*T*(2)–O> and <*T*(3)–O> distances is shown in Figure 7c. At the *I*4/m → $P4_2/n$ transition in marialite, the *T*(2) site splits into the *T*(2) and *T*(3) sites, with Al preferentially ordered at *T*(2) and Si preferentially ordered at *T*(3). This order reaches a maximum at Al ≈ 4.2 *apfu* and then decreases toward the composition of the $P4_2/n$ → *I*4/m transition in meionite. It will be shown later that this order of Al and Si over the *T*(2) and *T*(3) sites is never complete (see the ideal distances for complete occupancy by Al and Si indicated in Fig. 7c). Note that crystal S(14) deviates significantly from the trend of the rest of the data in Figure 7c. The structure refinement was repeated on another crystal from sample S(14), and the same result was obtained. Thus the deviation of S(14) from the trend in Figure 7c is real and statistically significant; this crystal shows more order of Al and Si over these two sites than the trend based on the other results suggests.

Assignment of site populations

For any framework aluminosilicate, one would normally use a relation analogous to that of Figure 6 to assign Al–Si site-occupancies. However, the situation is not so straightforward in scapolite. If a modified equation (1) is used to assign site occupancies, the *T*(1) site in *I*4/*m* marialite [crystals S(1)–S(6)] will be assigned significant (*i.e.*, ~0.30 *apfu*) Al. Above, we suggested two possibilities for the *T*(1) site in crystals S(1)–S(6): (1) there is no Al at *T*(1); (2) there is Al at *T*(1). If there is no Al at the *T*(1) site, relation (1) should extrapolate to the grand <*T*(1)–O> distance for crystals S(1)–S(6); the relevant values are as follows: grand <*T*(1)–O> = 1.6066(5) Å; extrapolated <*T*(1)–O> = 1.6027(6) Å. Similarly, if we extrapolate the trend for the *I*4/*m* structures to zero Al at *T*(1) [equation (5)], we get a <*T*(1)–O> distance of 1.6019(5) Å. The two extrapolated distances have a difference (and pooled standard deviation) of 0.0008(8) and hence are not significantly different. The grand <*T*(1)–O> distance for crystals S(1)–S(6) is 1.6066(5) Å, whereas the extrapolated distances for zero Al occupancy at *T*(1) are 1.6027(6) and 1.6019(5) Å; the difference between these values is 0.0039(8) Å = 4.9 σ, and hence is significant. These arguments *suggest* that a small amount of Al may occur at the *T*(1) site in *I*4/*m* marialite crystals S(1)–S(6). The alternative possibility is that the relation involving <*T*(1)–O>, <*T*(2)–O> and Al site-population is different in crystals S(1)–S(6) (*I*4/*m* marialite) and crystals S(7)–S(15) ($P4_2/n$ scapolite). How can we decide between these two possibilities?

Sokolova *et al*. (1996) and Sherriff *et al*. (1998, 2000) have examined *I*4/*m* marialite, $P4_2/n$ scapolite and *I*4/*m* meionite by ^{24}Si MAS and ^{27}Al SATRAS (SAtellite TRAnSition) NMR spectroscopy. From their fitted ^{29}Si MAS NMR spectra for *I*4/*m* marialite, Sokolova *et al*. (1996) stated that "There are 4.00 Si *apfu* in the *T*(1) sites for all three samples, within experimental error...". If there is Al at *T*(1) in samples of *I*4/*m* marialite, the <*T*(1)–O> distances in S(1)–S(6), together with the equations given above, indicate that there is ~ 0.31 Al *apfu* at *T*(1) . This amounts to a difference in spectral intensity of ~10% for each of the peaks assigned to Si at *T*(1); inspection of the fitted spectrum of PAM–1 (Sokolova *et al*. 1996, Fig. 4) [= S(1)] indicates that such a discrepancy is not possible. Hence we are left with a conundrum: Figure 8 and equations (1) and (5) suggest that Al occurs at *T*(1) in *I*4/*m* marialite, whereas the ^{29}Si MAS NMR spectrum indicates that Al does not occur at *T*(1) in these structures.

Let us approach this problem in a different way. The ^{29}Si MAS NMR results of Sokolova *et al*. (1996) indicate that there is no Al at *T*(1) in marialite sample PAM–1 [= S(1)]. As <*T*(1)–O> is the same in crystals S(1)–S(6), there is no Al at *T*(1) in crystals S(1)–S(6) [this is more in line with the grand <*T*(1)–O> distance of 1.6066(5) Å, which is closer to the <Si–O> distance of 1.609 Å in alpha quartz (*e.g*., Kihara 1990)]. If there is no Al at *T*(1), Figure 7 indicates that the relation between <*T*–O> in crystals S(1)–S(6) must be significantly different from the analogous relation in crystals S(7)–S(15). Possibly these different relations can be ascribed to the unusual response of the cell volume to increasing *Me* content for crystals S(1)–S(6) (see later discussion). Alternatively, the relation between <*T*–O> and Al–Si site-occupancy may differ for the *I*4/*m* and $P4_2/n$ scapolites; this is in line with equations (3) and (5), which are significantly different. Taking the Al occupancy of *T*(1) as zero for the *I*4/*m* marialite structures S(1)–S(6), we may plot the variation in <*T*(1)–O> and <*T*(2)–O> as a function of Al occupancy (Fig. 8a) and develop the following regression equation for prediction of Al site-occupancies in *I*4/*m* marialite:

$$\mathrm{Al} = 7.26(3) \langle T\text{–O}\rangle - 11.66(4) \quad \sigma = 0.0027,\ R^2 = 0.999 \qquad (12)$$

Next, we will use this equation to predict site occupancies for the *T*(1) and *T*(2) sites in *I*4/*m* meionite; if these values are correct, they must sum to the bulk composition of the crystal for each structure [note that data for crystals S(16)–S(18) were not used in developing equation (12)]. The predicted total Al contents for crystals S(16)–S(18) deviate from the analyzed values by 0.203, 0303 and 0.285 Al *apfu* [compared with a mean deviation of 0.013 Al *apfu* for crystals S(1)–S(6)]. Thus equation (12) is not an adequate equation for the prediction of Al site-occupancies in *I*4/*m* meionite.

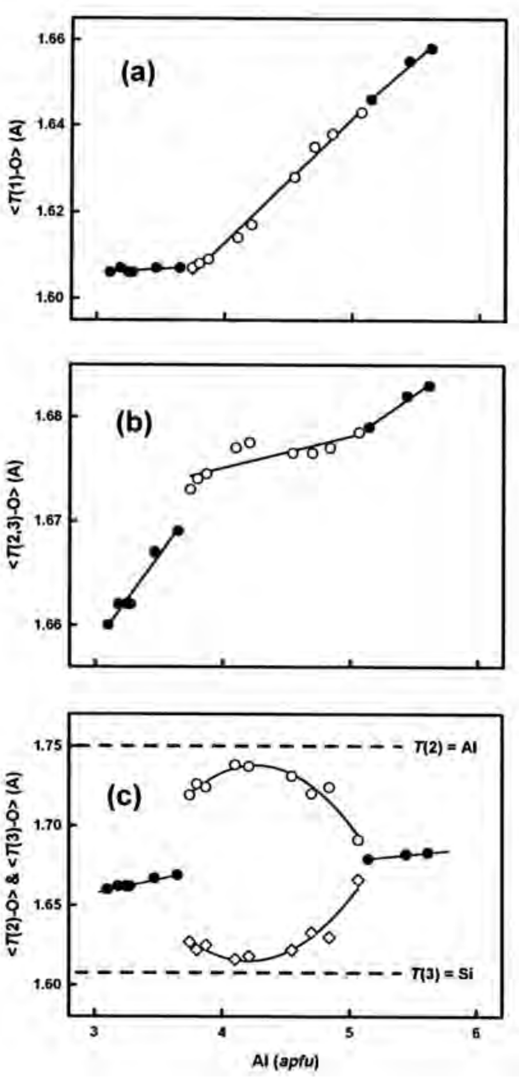

FIG. 7. Variation in mean <*T*–O> distances in the crystal structure of scapolite as a function of Al *apfu*: (a) <*T*(1)–O> distance; (b) <*T*(2)–O> (*I*4/*m*) and <*T*(2,3)–O> ($P4_2/n$) distances; (c) <*T*(2)–O> and <*T*(3)–O> distances ($P4_2/n$ only). Rhombs correspond to *T*(3) sites. Legend as in Figure 6.

TABLE 7. SELECTED INTERATOMIC DISTANCES (Å) AND ANGLES (°) FOR THE SCAPOLITE-GROUP MINERALS IN *I*4/*m*

		S(1)	S(2)	S(3)	S(4)	S(5)	S(6)	S(16)	S(17)	S(18)
T(1)–O(1)		1.599(1)	1.599(1)	1.598(1)	1.599(1)	1.599(2)	1.598(2)	1.623(1)	1.630(2)	1.630(2)
T(1)–O(1)′		1.603(1)	1.604(1)	1.605(1)	1.604(1)	1.604(2)	1.604(2)	1.629(2)	1.633(2)	1.636(2)
T(1)–O(4)	×2	1.611(1)	1.612(1)	1.611(1)	1.611(1)	1.613(1)	1.613(1)	1.665(1)	1.678(1)	1.682(1)
<*T*(1)–O>		1.606	1.607	1.606	1.606	1.607	1.607	1.646	1.655	1.658
T(2)–O(2)		1.661(1)	1.662(1)	1.662(1)	1.663(1)	1.666(1)	1.668(1)	1.675(1)	1.677(1)	1.678(1)
T(2)–O(3)		1.651(1)	1.652(1)	1.653(1)	1.653(1)	1.656(1)	1.659(1)	1.677(1)	1.681(1)	1.682(1)
T(2)–O(3)′		1.657(1)	1.659(1)	1.660(1)	1.661(1)	1.665(1)	1.667(1)	1.678(1)	1.680(1)	1.682(2)
T(2)–O(4)		1.672(1)	1.673(1)	1.674(1)	1.675(1)	1.679(1)	1.683(1)	1.687(1)	1.688(1)	1.689(1)
<*T*(2)–O>		1.660	1.662	1.662	1.663	1.667	1.669	1.679	1.682	1.683
M–O(2)		2.386(2)	2.377(2)	2.377(2)	2.373(2)	2.354(2)	2.342(2)	2.353(2)	2.356(2)	2.355(2)
M–O(3)	×2	2.558(1)	2.550(1)	2.549(1)	2.543(1)	2.525(1)	2.512(1)	2.504(1)	2.503(1)	2.501(1)
M–O(4)	×2	2.912(1)	2.910(1)	2.912(1)	2.912(1)	2.871(2)	2.843(2)	2.695(1)	2.677(2)	2.669(1)
M–O(4)′	×2	2.949(1)	2.927(1)	2.928(1)	2.917(2)	2.908(1)	2.905(1)	2.894(1)	2.890(1)	2.889(1)
<*M*–O>		2.746	2.736	2.733	2.731	2.709	2.695	2.648	2.642	2.639
M–*A*		2.927(1)	2.945(1)	2.947(1)	2.956(1)	2.995(1)	3.021(1)	3.164(1)	3.191(1)	3.196(1)
M–O(7)a		–	–	–	–	–	2.30(7)	2.44(2)	2.46(4)	2.48(4)
M–O(7)b		–	–	–	–	–	2.27(7)	2.35(3)	2.30(4)	2.33(4)
M–O(8)a		–	–	–	–	–	2.83(8)	3.23(7)	2.78(8)	2.8(1)
M–O(8)c		–	–	–	–	–	2.00(4)	2.10(2)	2.25(3)	2.21(5)
M–O(9)d		–	–	–	–	–	–	2.06(3)	2.14(3)	2.10(2)
M–O(9)b		–	–	–	–	–	–	2.73(4)	2.95(7)	3.0(1)
M–O(10)e	×2	–	–	–	–	–	2.32(7)	2.57(1)	–	–
M–O(10)f	×2	–	–	–	–	–	2.5(1)	2.55(1)	–	–
T(1)–O(1)–*T*(1)′		159.1(1)	159.1(1)	159.1(1)	159.1(1)	159.1(1)	159.3(1)	157.3(1)	156.8(1)	156.6(1)
T(2)–O(2)–*T*(2)′		140.72(9)	140.6(1)	140.57(9)	140.5(1)	140.2(1)	139.8(1)	138.83(9)	138.8(1)	138.8(1)
T(2)–O(3)–*T*(2)′		149.09(7)	148.96(8)	148.98(7)	148.79(8)	148.42(8)	148.07(8)	145.57(7)	145.29(9)	145.24(7)
T(1)–O(4)–*T*(2)		138.36(6)	138.33(7)	138.33(7)	138.28(7)	138.03(8)	137.89(8)	136.43(7)	135.87(8)	135.71(7)
<*T*–O–*T*>		146.8	146.7	146.7	146.7	146.4	146.3	144.5	144.2	144.1
C–O(7)		–	–	–	–	–	–	1.32(3)	1.32(2)	1.32(2)
C–O(8)		–	–	–	–	–	–	1.28(3)	1.26(2)	1.26(2)
C–O(9)		–	–	–	–	–	–	1.27(3)	1.26(2)	1.26(2)
<*C*–O>		–	–	–	–	–	–	1.29	1.28	1.28
O(7)–*C*–O(8)		–	–	–	–	–	–	119.74(2.71)	115.52(2.16)	114.45(1.98)
O(7)–*C*–O(9)		–	–	–	–	–	–	115.66(2.50)	117.13(2.36)	116.94(2.03)
O(8)–*C*–O(9)		–	–	–	–	–	–	124.60(3.14)	127.35(2.31)	128.60(2.08)
<O–*C*–O>		–	–	–	–	–	–	120.00	120.00	120.00

a: –x + 1/2, –y + 1/2, –z + 1/2; b: y + 1/2, –x + 1/2, –z + 1/2; c: –y + 1/2, x + 1/2, z – 1/2; d: x – 1/2, y – 1/2, z + 1/2; e: x + 1/2, y + 1/2, z – 1/2; f: y + 1/2, –x + 1/2, z – 1/2.

Now we need to develop a similar relation to predict the Al site-occupancies of the *T*(1), *T*(2), and *T*(3) sites in $P4_2/n$ scapolites S(7)–S(15). The only way we can do this is to assume that *T*(1), *T*(2) and *T*(3) respond in the same fashion to variations in site occupancy. With this constraint, we may plot the mean Al site-occupancy as a function of the mean <*T*–O> distance, and use the resultant relation for the individual sites. This variation is shown in Figure 8b, and the resulting regression equation is as follows:

$$\mathrm{Al} = -11.37(17) + 7.075(102)\ \langle T\text{–O}\rangle$$
$$\sigma = 0.0016,\ R^2 = 0.999 \qquad (13)$$

For crystals S(16)–S(18), we similarly assume that the relation between occupancy and <*T*–O> distance is the same for the *T*(1) and *T*(2) sites. The resulting regression equation is as follows:

$$\mathrm{Al} = -9.6(1.0) + 6.0(4)\ \langle T\text{–O}\rangle$$
$$\sigma = 0.0029,\ R^2 = 0.989 \qquad (14)$$

Site populations assigned from these equations are given in Table 9 for scapolites S(1)–S(18). The site occupancies are given to three decimal places, as the standard errors of estimates for each of the regression equations [(12), (13) and (14)] are in the third decimal place. In addition, the rank of the equipoints for each site is 4, and one must be careful in avoiding termination errors when calculating the total Al content of each crystal from the site occupancies. A comparison of the latter values with the values from the unit formulae derived from the chemical compositions (Table 4) is

TABLE 8. SELECTED INTERATOMIC DISTANCES (Å) AND ANGLES (°) FOR THE SCAPOLITE-GROUP MINERALS IN $P4_2/n$

	S(7)	S(8)	S(9)	S(10)	S(11)	S(12)	S(13)	S(14)	S(15)
T(1)–O(1)	1.601(1)	1.601(1)	1.604(1)	1.604(1)	1.608(1)	1.614(1)	1.618(1)	1.621(1)	1.622(1)
T(1)–O(1)′	1.603(1)	1.604(1)	1.604(1)	1.608(1)	1.608(1)	1.615(1)	1.620(1)	1.620(1)	1.626(1)
T(1)–O(6)	1.619(1)	1.623(1)	1.623(1)	1.633(1)	1.637(1)	1.654(1)	1.658(2)	1.663(1)	1.663(2)
T(1)–O(5)	1.603(1)	1.603(1)	1.604(1)	1.609(1)	1.613(1)	1.630(1)	1.643(2)	1.646(1)	1.662(2)
<*T*(1)–O>	1.607	1.608	1.609	1.614	1.617	1.628	1.635	1.638	1.643
T(2)–O(2)	1.716(1)	1.725(1)	1.722(1)	1.736(1)	1.734(1)	1.728(1)	1.718(2)	1.721(1)	1.690(2)
T(2)–O(3)	1.720(2)	1.725(1)	1.722(1)	1.735(1)	1.735(1)	1.730(1)	1.715(2)	1.723(1)	1.687(2)
T(2)–O(4)	1.709(2)	1.716(1)	1.717(1)	1.732(1)	1.730(1)	1.728(1)	1.718(2)	1.723(1)	1.689(2)
T(2)–O(5)	1.732(1)	1.738(1)	1.736(1)	1.748(1)	1.747(1)	1.738(1)	1.727(2)	1.730(1)	1.698(2)
<*T*(2)–O>	1.719	1.726	1.724	1.738	1.737	1.731	1.720	1.724	1.691
T(3)–O(2)	1.620(1)	1.615(1)	1.618(1)	1.608(1)	1.611(1)	1.617(1)	1.626(1)	1.624(1)	1.658(2)
T(3)–O(3)	1.614(2)	1.611(1)	1.615(1)	1.607(1)	1.609(1)	1.616(1)	1.629(2)	1.625(1)	1.665(2)
T(3)–O(4)	1.620(1)	1.613(1)	1.614(1)	1.605(1)	1.608(1)	1.612(1)	1.626(2)	1.623(1)	1.664(2)
T(3)–O(6)	1.652(1)	1.647(1)	1.651(1)	1.642(1)	1.642(1)	1.643(1)	1.650(2)	1.647(1)	1.677(2)
<*T*(3)–O>	1.627	1.622	1.625	1.616	1.618	1.622	1.633	1.630	1.666
M–O(2)	2.358(2)	2.353(2)	2.352(2)	2.345(1)	2.341(1)	2.351(1)	2.351(2)	2.349(1)	2.355(1)
M–O(3)	2.529(2)	2.530(1)	2.525(1)	2.519(1)	2.519(1)	2.523(1)	2.523(2)	2.522(1)	2.507(2)
M–O(4)	2.496(2)	2.494(1)	2.494(1)	2.489(1)	2.489(1)	2.498(1)	2.502(2)	2.498(1)	2.506(2)
M–O(5)	2.789(2)	2.776(2)	2.763(2)	2.719(2)	2.706(1)	2.682(1)	2.683(2)	2.664(1)	2.679(2)
M–O(5)′	2.840(2)	2.830(1)	2.838(2)	2.825(1)	2.818(1)	2.831(1)	2.823(2)	2.816(1)	2.882(2)
M–O(6)	2.895(2)	2.896(2)	2.882(2)	2.870(1)	2.850(1)	2.820(1)	2.786(2)	2.775(1)	2.721(2)
M–O(6)′	2.991(1)	2.997(1)	2.984(1)	2.986(1)	2.983(1)	2.962(1)	2.949(2)	2.952(1)	2.905(2)
<*M*–O>	2.700	2.697	2.691	2.679	2.672	2.667	2.660	2.654	2.651
M–*A*	3.035(1)	3.043(1)	3.054(1)	3.083(1)	3.098(1)	3.124(1)	3.141(1)	3.150(0)	3.159(0)
M–O(7)a	2.41(5)	2.47(9)	2.45(6)	2.46(4)	2.47(2)	2.36(2)	2.42(2)	2.63(2)	2.44(2)
M–O(7)b	2.21(5)	1.94(7)	2.08(5)	2.17(3)	2.17(2)	2.30(2)	2.27(2)	2.15(1)	2.25(3)
M–O(8)a	–	2.38(8)	2.6(1)	2.54(6)	2.58(3)	2.93(6)	2.77(5)	2.53(2)	2.74(6)
M–O(8)c	–	2.19(9)	2.15(6)	2.24(4)	2.17(3)	2.11(3)	2.16(3)	2.28(1)	2.23(3)
M–O(9)d	–	2.08(9)	1.97(5)	1.95(3)	1.90(2)	2.08(2)	2.04(2)	2.00(2)	2.11(2)
M–O(9)b	–	3.0(1)	3.0(1)	3.1(1)	3.16(5)	2.79(4)	2.91(4)	3.31(5)	2.89(4)
M–O(10)b	2.29(5)	2.32(4)	2.30(5)	–	–	–	–	–	2.56(3)
M–O(10)a	2.38(6)	2.43(5)	2.46(6)	–	–	–	–	–	2.56(3)
M–O(11)b	2.34(4)	2.44(3)	2.45(3)	2.41(2)	2.43(3)	2.49(2)	–	–	2.56(3)
M–O(11)a	2.45(5)	2.43(4)	2.53(3)	2.50(2)	2.52(3)	2.53(3)	–	–	2.67(3)
T(1)–O(1)–*T*(1)′	159.5(1)	159.41(9)	159.3(1)	159.3(1)	159.0(1)	158.39(9)	158.1(1)	157.93(8)	157.51(9)
T(2)–O(2)–*T*(3)	139.7(1)	139.34(8)	139.23(9)	138.84(9)	138.71(9)	138.70(8)	138.56(9)	138.45(7)	138.96(8)
T(2)–O(3)–*T*(3)	146.8(1)	146.60(8)	146.42(9)	145.63(9)	145.57(8)	145.29(8)	145.4(1)	145.10(8)	145.4(1)
T(2)–O(4)–*T*(3)	148.3(1)	148.36(8)	148.05(9)	147.63(9)	147.44(8)	146.96(8)	146.4(1)	146.24(8)	146.0(1)
T(1)–O(5)–*T*(2)	137.53(9)	137.45(8)	137.54(8)	137.32(8)	137.15(8)	136.85(8)	136.6(1)	136.29(7)	136.5(1)
T(1)–O(6)–*T*(3)	138.48(9)	138.41(8)	138.34(8)	138.17(8)	138.06(8)	137.59(8)	137.4(1)	137.24(7)	136.5(1)
<*T*–O–*T*>	145.05	144.94	144.81	144.48	144.32	143.96	143.74	143.54	143.48
C–O(7)	–	1.34(2)	1.30(2)	1.30(2)	1.33(3)	1.30(3)	1.34(3)	1.30(3)	1.32(3)
C–O(8)	–	1.34(2)	1.31(2)	1.30(2)	1.32(3)	1.28(3)	1.31(3)	1.28(3)	1.29(3)
C–O(9)	–	1.34(2)	1.25(2)	1.25(3)	1.30(3)	1.28(3)	1.30(3)	1.29(3)	1.27(3)
<*C*–O>	–	1.34	1.29	1.28	1.32	1.29	1.32	1.29	1.29
O(7)–*C*–O(8)	–	120(2)	117(3)	109(3)	112(2)	112(3)	112(2)	116(2)	115(3)
O(7)–*C*–O(9)	–	120(3)	121(4)	121(4)	123(3)	118(2)	115(3)	120(2)	117(3)
O(8)–*C*–O(9)	–	120(3)	121(3)	124(5)	125(3)	121(3)	126(3)	124(3)	127(3)
<O–*C*–O>	–	120	120	118	120	119	118	120	120

a: –x + 1/2, –y + 1/2, z; b: y, –x + 1/2, –z + 3/2; c: –y + ½, x, –z + 3/2; d: x, y, z.

shown in Figure 9. The standard errors of estimates for the $I4/m$ marialite, $P4_2/n$ scapolite, and $I4/m$ meionite series are 0.032, 0.019 and 0.035 Al *apfu*, respectively, and none of the data deviate significantly from the 1:1 line in Figure 9.

Lin (1975) suggested a highly ordered Al–Si distribution between $T(2)$ and $T(3)$ at a composition [$Al_4Si_8O_{24}$], *i.e.*, with an Si/Al ratio of 2:1. Of all eighteen samples, S(10) and S(11), with Si/Al ratios of 1.92:1 and 1.85:1, respectively, are the mostly highly ordered scapolites, exhibiting maximal difference between $<T(2)–O>$ and $<T(3)–O>$ distances. From equation (13), we may extrapolate to zero and full occupancy of Al; the resultant values are as follows: <Si–O> = 1.6071(16), <Al–O> = 1.7484(16) Å. Thus for crystals S(10) and S(11) with maximal Al–Si order, the $<T(2)–O>$ and $<T(3)–O>$ distances, 1.728 and 1.617 Å, respectively, show that there is still some small amount of disorder of Al over the $T(2)$ and $T(3)$ sites (Fig. 7c). Of the $P4_2/n$ scapolites, S(15) has the maximum Si/Al disorder observed, with $<T(2)–O>$ 1.691 and $< T(3)–O>$ 1.666 Å. For this crystal, only three reflections violate the condition $h + k + l = 2n$ ($F_o > 4\sigma F$), and the composition must correspond almost exactly to that at the $I4/m \rightarrow P4_2/n$ second-order phase transition.

Long-range order–disorder of Al and Si

The order of Al over the $T(1)$ and $T(2) + T(3)$ sites as a function of total Al content is shown in Figure 10; the line joining Me_0 (dis) and Me_{100} (dis) shows the relation for total Al–Si disorder between the marialite and meionite end-member compositions. First, it is notable that meionite shows a much higher degree of Al–Si order than marialite. Second, the data of Figure 10 indicate that there is some residual order at the end-member meionite composition: the trends in site occupancies for $T(1)$ and $T(2)$ do not (linearly) extrapolate to complete disorder [Me_{100} (dis) in Fig. 10] [of course, the trends may nonlinearly converge to Me_{100} (dis) in the region $Me_{>93}$.

THE *M* SITE

The refined site-scattering values at the M site are given in Table 10, together with the site populations assigned from the unit formulae calculated from the electron-microprobe data. There is close agreement between the refined site-scattering values and those calculated from the electron-microprobe data (Fig. 11a, $R^2 = 0.996$), indicating that there is no significant systematic error in either of the two sets of results. Figure 11b shows the variation in <M–O> as a function of constituent-cation radius (values from Shannon 1976), where the O anions belong to the aluminosilicate framework [*i.e.*, no anions of the (CO_3) group or the Cl anion are included]. There are two distinct trends for the $I4/m$ and $P4_2/n$ structures, the former having a distinctly steeper slope. In the crystal structure of

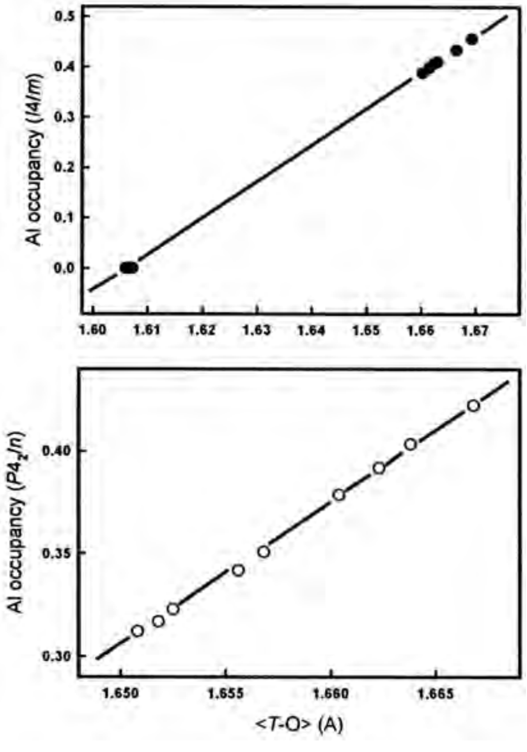

FIG. 8. Variation in Al occupancy as a function of $<T–O>$ in scapolites: (a) $<T(1)–O>$ and $<T(2)–O>$ in $I4/m$ marialite [crystals S(1)–S(6)]; (b) $<T–O>$ in $P4_2/n$ scapolite [crystals S(7)–S(15)]; legend as in Figure 6.

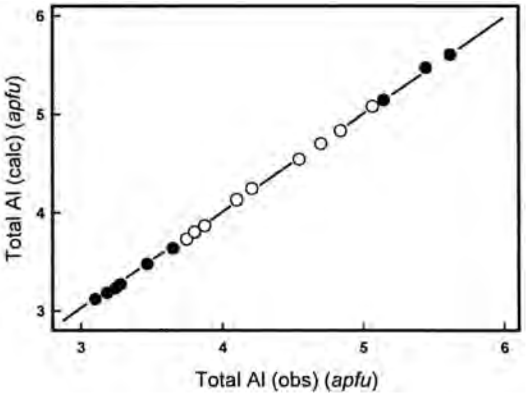

FIG. 9. Comparison of the observed Al content (*apfu*) with the Al content calculated from equations (12), (13) and (14) for both $I4/m$ and $P4_2/n$ scapolites; legend as in Figure 6.

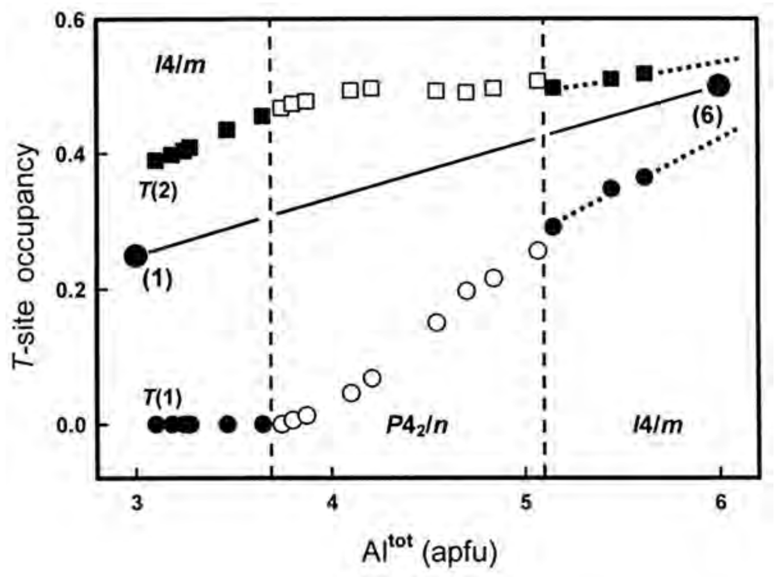

FIG. 10. Variation in Al occupancy of the *T*(1) and *T*(2) [≡ *T*(2) + *T*(3) in $P4_2/n$ crystals] as a function of total Al content; the large black circles denote complete disorder for (1) end-member marialite and (2) end-member meionite; legend as in Figure 6.

TABLE 9. ASSIGNED *T*-SITE OCCUPANCIES IN SCAPOLITE-GROUP MINERALS

	$^{T(1)}$Al	$^{T(1)}$Si	$^{T(2)}$Al	$^{T(2)}$Si	$^{T(3)}$Al	$^{T(3)}$Si
S(1)	0.00	1.00	0.390	0.610	–	–
S(2)	0.00	1.00	0.398	0.602	–	–
S(3)	0.00	1.00	0.404	0.596	–	–
S(4)	0.00	1.00	0.409	0.591	–	–
S(5)	0.00	1.00	0.435	0.565	–	–
S(6)	0.00	1.00	0.455	0.545	–	–
S(7)	0.00	1.00	0.795	0.205	0.138	0.862
S(8)	0.006	0.994	0.842	0.158	0.103	0.897
S(9)	0.013	0.987	0.830	0.170	0.124	0.876
S(10)	0.046	0.954	0.926	0.074	0.060	0.940
S(11)	0.068	0.932	0.917	0.083	0.075	0.925
S(12)	0.151	0.849	0.878	0.122	0.106	0.894
S(13)	0.197	0.803	0.796	0.204	0.183	0.817
S(14)	0.216	0.784	0.830	0.170	0.162	0.838
S(15)	0.257	0.743	0.595	0.405	0.418	0.582
S(16)	0.292	0.708	0.497	0.503	–	–
S(17)	0.348	0.652	0.510	0.490	–	–
S(18)	0.365	0.635	0.518	0.482	–	–

TABLE 10. FINAL ASSIGNED *M*-SITE POPULATIONS

	Site population (*apfu*)			Site scattering (*epfu*)	
	Na	Ca*	K	SREF	EMPA
S(1)	3.52	0.20	0.28	48.0	48.1
S(2)	3.47	0.30	0.23	48.5	48.6
S(3)	3.44	0.31	0.25	49.1	48.8
S(4)	3.42	0.36	0.22	49.2	49.0
S(5)	3.29	0.60	0.11	51.0	50.3
S(6)	3.11	0.84	0.05	51.3	52.0
S(7)	2.68	1.06	0.26	55.8	55.6
S(8)	2.58	1.15	0.27	55.7	56.5
S(9)	2.50	1.29	0.21	57.2	57.3
S(10)	2.15	1.68	0.17	60.0	60.5
S(11)	2.08	1.83	0.09	59.7	61.2
S(12)	1.57	2.30	0.13	66.4	65.7
S(13)	1.26	2.67	0.07	67.9	68.6
S(14)	1.19	2.78	0.03	68.8	69.3
S(15)	0.89	3.07	0.04	72.4	72.0
S(16)	0.85	3.13	0.02	72.9	72.3
S(17)	0.33	3.53	0.14	77.1	76.9
S(18)	0.19	3.71	0.10	79.7	78.2

* Ca = Ca + Fe^{2+} + Sr.

end-member marialite, the coordination number of the M atom is eight. Seven ligands are O atoms of the Si–Al framework, and the eighth ligand is a Cl atom (Fig. 12a). In $P4_2/n$, the O(4) site splits into O(5) and O(6) sites: the *M*–O(5,6) bonds are invariably shorter than the *M*–O(5,6)' bonds, and there is correspondence between O(4) and O(5), O(6) and O(4)' and O(5)', O(6)', comparing *M*–O bonds in *I*4/*m* and $P4_2/n$ (Tables 8, 9). Figure 12 shows the possible short-range arrangements of anions about the *M* site. Where the *A* site is occupied by Cl (Fig. 12a), the coordination number of the M cation is [8]. Where the *A* cavity is occupied by (SO_4) (Fig. 12b), the coordination number of the cation is [9]. Where the *A* cavity is occupied by (CO_3), the coordination number of the M cation can be [8] (Figs. 12c, d) or [9] (Figs. 12e, f), depending on the local arrangement. Thus in end-member marialite, the M cation is [8]-coordinated; in end-member meionite, the M cation is (on average) [8.5]-coordinated.

In the structure of scapolite, the M polyhedra share common edges to form columns extending along [001] (Fig. 13a). These columns connect to each other through common vertices (occupied by the A anions) to form sheets that extend along [110] and [$\bar{1}$10], and these sheets link *via* common vertices occupied by the A anions (Fig. 13b). This arrangement is designated as the M framework.

THE *A* SITE

The *A* site is located in a type-1 channel. It is occupied dominantly by Cl in marialite, S(1)–S(9), with $0.98 \geq \text{Cl} \geq 0.62$ *apfu* (Table 4). As the *A* site is surrounded by four M atoms, the Cl atom is bonded to four (usually Na) atoms. With increasing *Me* content, Cl is replaced by (CO_3) and (SO_4) anions at the *A* site, and in meionite, divalent anions are dominant at the *A* site: for S(10)–S(18) $0.38 \leq (CO_3) \leq 0.94$ *apfu* and $0.52 \leq (CO_3 + SO_4) \leq 0.97$ *apfu*. Sulfur replaces Cl at the *A* site, whereas C occupies four disordered sites positionally displaced from the *A* site. Our refinements confirm the disordered models for the (CO_3) and (SO_4) groups (Papike & Stephenson 1966, Levien & Papike 1976, Peterson *et al.* 1979) and show that they are applicable to all compositions across the marialite–meionite solid-solution series.

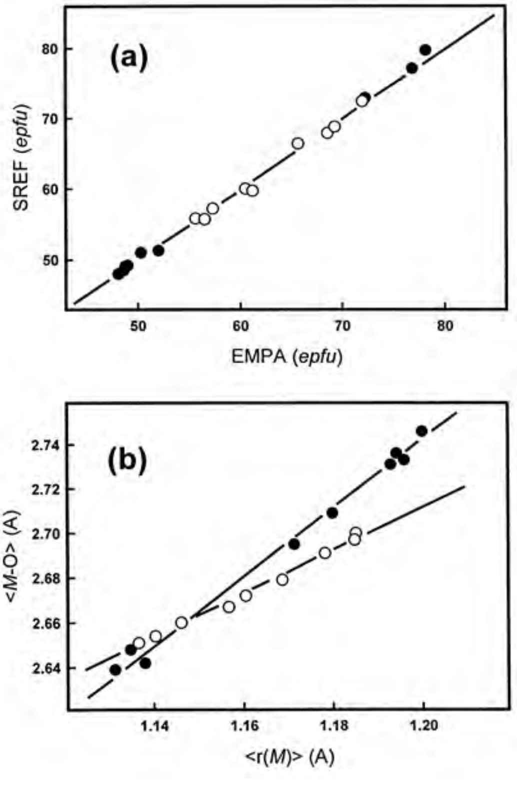

FIG. 11. (a) Comparison of the site-scattering values (*epfu*) for the *M* site from site refinement (SREF) and electron-microprobe data (EMPA); (b) variation in <*M*–O> as a function of constituent-cation radius at the *M* site shown as two linear trends, one for *I*4*m* scapolite (black circles) and one for $P4_2/n$ scapolite (white circles).

The (CO_3) group

There are four (CO_3) groups in the (001) plane arranged about the 4 axis (*I*4/*m*) or $\bar{4}$ axis ($P4_2/n$). Each (CO_3) triangle is bonded to four M atoms, and one local arrangement is shown in Figure 14; there are four (equivalent) orientations for this arrangement. Corresponding *M*–O(7,8,9) bonds are listed in Tables 7 and 8. Where a specific M cation has one bond to the (CO_3) group, this bond is short and varies between 2.00 and 2.25 Å in *I*4/*m* and between 1.90 and 2.28 Å in $P4_2/n$. Where a specific M cation has two bonds to the (CO_3) group [*i.e.*, the (CO_3) and (MO_9) polyhedra share a common edge], the *M*–O bonds involving the O atoms constituting the common edge are longer than those to a single O atom. Note that each O atom of the carbonate group is bonded to two M atoms and thus is [3]-coordinated.

The sulfate group

In *I*4/*m*, the (SO_4) group occurs in two distinct orientations (related by 90° rotation around the 4-fold axis) in equal amounts. However, it is not clear if there are deviations from this relation, as the sulfate contents of these (and most) scapolites are low, and such deviations may have a negligible effect on the diffraction of the X-rays. In $P4_2/n$, there are also two distinct conformations of the (SO_4) group, but the long-range symmetry does not require that the two distinct conformations occur in equal amounts; in fact, Figure 5c indicates that these conformations *do not* occur in equal amounts.

LINKAGE OF *M* AND *T* POLYHEDRA

The crystal structure of scapolite can be described as two interpenetrating frameworks, the *T* framework and the *M* framework; interframework linkage is shown in Figure 15. Each M polyhedron is connected to three *T*(1) tetrahedra from different *T*(1) rings: it shares an edge with one tetrahedron and two vertices with the other two tetrahedra; this common edge is O(4)–O(4) (*I*4/*m*, Fig. 15a) or O(5)–O(6) ($P4_2/n$, Fig. 15b). Similarly, the *T*(1) tetrahedron is linked through a common edge to one M polyhedron, and through a common vertex to two M polyhedra: all three M polyhedra belong to the same

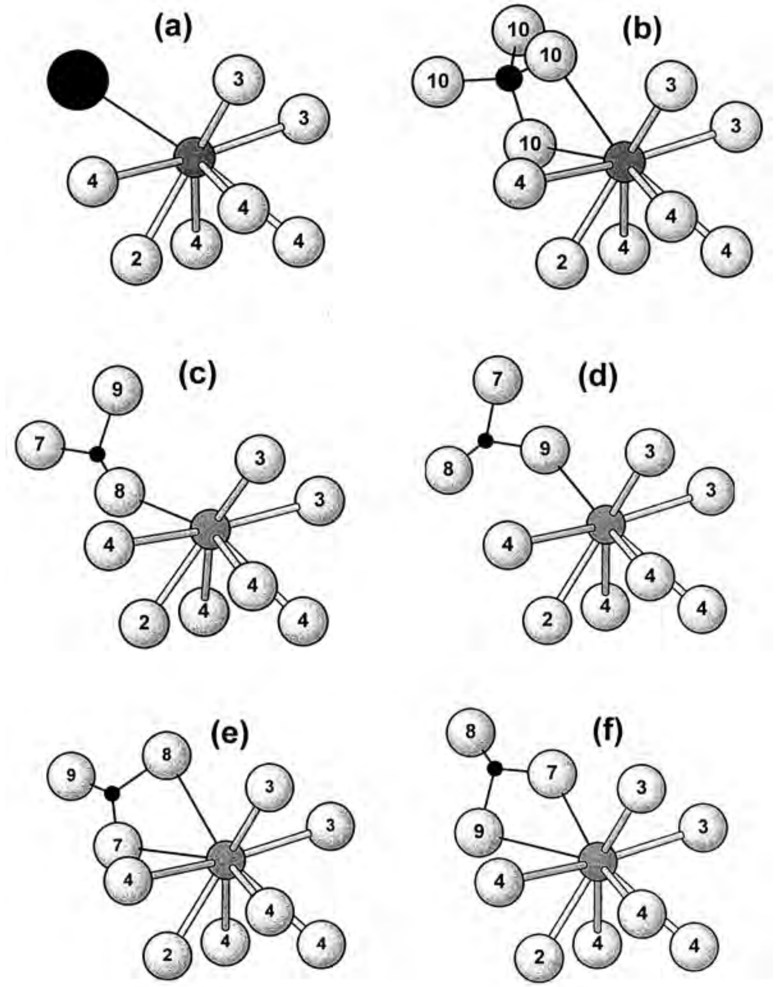

FIG. 12. Possible local arrangements of atoms around the *M* site (*I*4/*m*): (a) CN = [8] with seven framework O atoms and one Cl atom; (b) the M atom coordinated by two additional O atoms of the (SO_4) group; (c)–(f) coordination of the M cation by four different (CO_3) groups. The M cation is shown as a medium grey circle, the C, S and Cl atoms are shown as small, medium and large black circles, O atoms are shown as numbered shaded white circles.

column. Thus each column of M polyhedra is connected to two "sequences" of *T*(1) rings along [001]: there is edge-sharing with one *T*(1) sequence and corner-sharing with another *T*(1) "sequence". Each M polyhedron shares four common edges with four *T*(2) tetrahedra: two O(2)–O(4) edges and two O(3)–O(4) edges; two common vertices, O(3), are also shared with another two *T*(2) tetrahedra. Conversely, each *T*(2) tetrahedron shares two edges with two neighboring M polyhedra from one column and a vertex with an *M* polyhedron from another column. In $P4_2/n$, the *T*(2) site has split into the *T*(2) and *T*(3) sites, and the *M* polyhedron shares two common edges with two *T*(2) tetrahedra and two common edges with two *T*(3) tetrahedra: O(2)–O(5) and O(5)–O(4) for *T*(2), and O(2)–O(6) and O(6)–O(3) for *T*(3). The *T*(2) tetrahedron contains more Al and is larger than the *T*(3) tetrahedron. The tetrahedron edges O(2)–O(5) and O(5)–O(4) are about 0.1 Å longer than the edges O(2)–O(6) and O(6)–O(3). Corner-sharing of the *M* polyhedron with *T*(2) and *T*(3) tetrahedra of a different size requires matching of both fragments. As a result, the square face O(4)–O(4)–O(3)–O(3) (*I*4/*m*,

Fig. 15a) is broken in two triangular faces, O(5)–O(4)–O(6) and O(4)–O(3)–O(6) in $P4_2/n$ (Fig. 15b).

VARIATION IN CELL DIMENSIONS

Figure 16 shows the variation in cell dimensions as a function of Me_x for S(1)–S(18).

The a parameter

The increase in the *a* parameter across the series is 0.1627 Å, *i.e.*, about 1.4% of the minimal value of 12.0450 Å for S(6); the maximal *a* value is 12.2077 Å for S(18). Figure 16a shows a decrease in the *a* parameter for S(1)–S(6) with 3.103 < Al < 3.649 *apfu* from 12.0570 to 12.0450 Å. There is a linear increase in the *a* parameter for $P4_2/n$ scapolite from S(7) to S(15) with 3.745 < Al < 5.068 *apfu*, from 12.0720 to 12.1674 Å. The three *I*4/*m* scapolites, S(16)–S(18), also show an increase in the *a* parameter (from 12.1713 to 12.2077 Å).

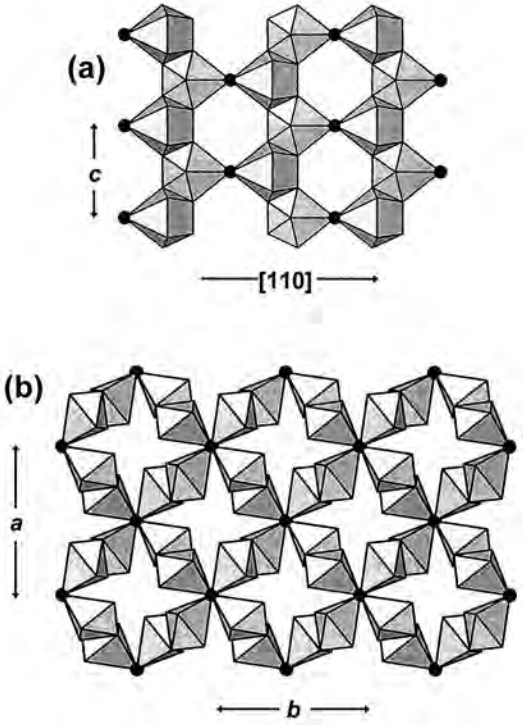

FIG. 13. The arrangement of [8]-coordinated *M* polyhedra in scapolite S(1): (a) projected onto (1$\bar{1}$0); (b) projected onto (001). The [8]-coordinated *M* polyhedra are grey, and Cl atoms are shown as black circles.

The c parameter

The increase in the *c* parameter across the series is 0.0197 Å, *i.e.*, about 2.6% of the minimal value of 7.5644 Å for S(1); the maximal *c* value is 7.5841 Å for S(10). Figure 16b shows changes in the *c* parameter as a function of Al content: *c* increases in *I*4/*m* marialite [S(1)–S(6)] (with 3.103 < Al < 3.649 *apfu*), decreases in the $P4_2/n$ scapolites [S(7)–S(15) with 3.745 < Al < 5.068 *apfu*], and increases again for the *I*4/*m* meionite [S(16)–S(18) with 5.147 < Al < 5.617 *apfu*].

Cell volume

Variation in cell volume across the series is shown in Figure 16c. The variation in *V* as a function of composition is similar to the analogous variation in *a* (Fig. 16a), except in *I*4/*m* marialite [S(1)–S(6)]. In that particular part of the solid solution, the *a* parameter decreases and the *c* parameter increases; coupling of these two trends results in no change in the cell volume.

Previous work on cell dimensions in scapolite has emphasized two points: (1) increase in Al content and expansion of the *T*-framework, and (2) cooperative rotation of tetrahedra; neither of these factors was regarded as dominant. Cooperative rotation of tetrahedra causes contraction of the oval channels with increasing *Me* content (or corresponding increase of Al content) (Papike & Stephenson 1966). Increase in Al content results in expansion of *T* tetrahedra constituting the framework. There are distinct similarities between Figures 16a, b and 7a, b. Variation in <*T*(1)–O> corre-

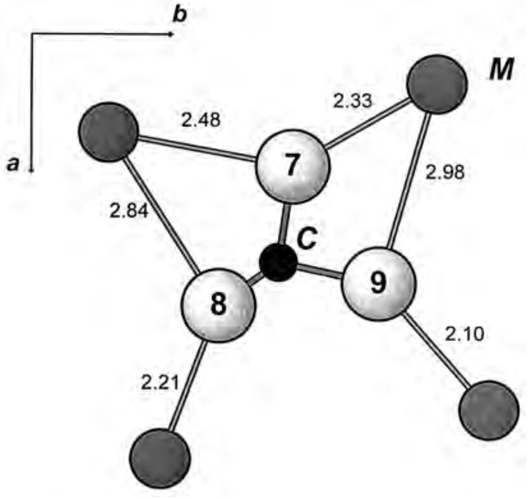

FIG. 14. The coordination of the (CO_3) group in the *A* cage in crystal S(18); the M cation is shown by a grey circle, the C atom is shown by a black circle, the oxygen atoms O(7), O(8) and O(9) of the carbonate group are shown as pale grey circles; interatomic distances are shown in Å.

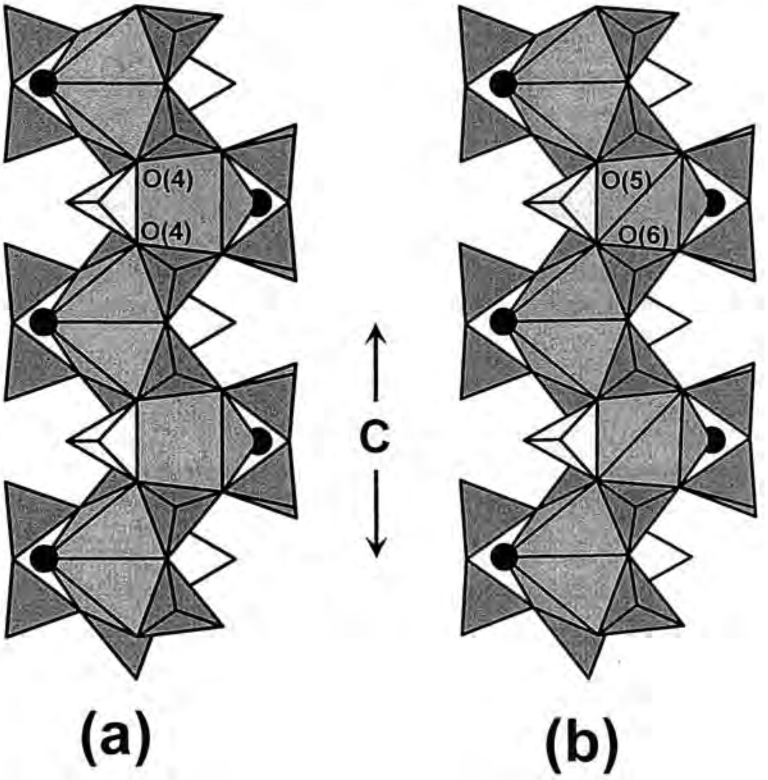

FIG. 15. A fragment of the crystal structure of scapolite showing linkage of *M* polyhedra and *T* tetrahedra: (a) *I*4/*m*; (b) *P*4$_2$/*n*. Polyhedra: *T*(1): very pale grey; *T*(2) and *T*(3): dark grey; Ca: medium grey; Cl: black circle.

lates well with the variation in *a* (Figs. 7a, 16a), and variation in the <*T*(2,3)–O> correlates well with the variation in *c* (Figs. 7b, 16b).

The *a* cell-parameter decreases slightly in *I*4/*m* marialite (Fig. 16a) as Al increases from 3.103 to 3.649 *apfu* and (CO_3) changes from 0.010 to 0.128 *apfu*. The Al atom does not occur at the *T*(1) site (Fig. 7a); it occurs at the *T*(2) site, and the <*T*(2)–O> distance increases with increasing Al^{TOT}. With (CO_3) replacing Cl at the *A* site, the <*M*–*A*> distance increases rapidly (Tables 7, 8). If <*T*(2)–O> and <*M*–*A*> both increase with increasing Al content, why doesn't the *a* cell-parameter increase as well? It does not increase because of rotation of tetrahedra. Figures 17a and 17b show variations in the angle α *versus* content of Al (*apfu*) and the *a* cell-parameter, where α is the angle between the diameters of the *T*(1) and *T*(2) rings. The α angle decreases rapidly where <*T*(2)–O> and <*M*–*A*> increase. As a result, the *a* cell-parameter does not change. The α angle cannot decrease in the way that it does for *I*4/*m* marialite because it would lead to contraction of channels. Where (CO_3) replaces Cl and Ca replaces Na, *M*–O bonds change: the longer bonds to the *T*(1) tetrahedron become shorter and the shorter bonds to the oxygen atoms of the *T*(2) site become longer, decreasing on average. This change is possible because Al enters the *T*(1) site upon change in space group; <*T*(1)–O> increases rapidly, affecting the length of the *a* cell parameter. Where both diameters of the *T*(1) and *T*(2) rings increase, the rate of change of the α angle is less than in *I*4/*m* marialite (Figs. 17a,b).

SUMMARY

(1) There are different relations between <*T*–O> distances and Al–Si site-populations in *I*4/*m* marialite and *P*4$_2$/*n* scapolite and *I*4/*m* meionite:

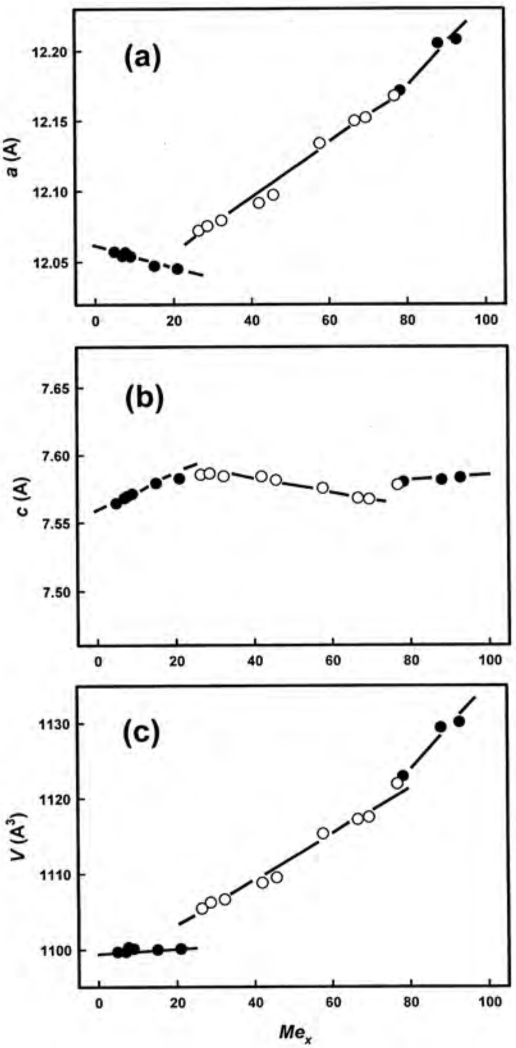

FIG. 16. Variation in *a*, *c* and *V* as a function of Me_x in the marialite–meionite series; legend as in Figure 6.

$I4/m$ marialite: Al = 7.26(3) $<T–O>$ – 11.66(4)
$\sigma = 0.0027$, $R^2 = 0.999$

$P4_2/n$ scapolite: Al = 7.075(102) $<T–O>$ – 11.37(17) $\sigma = 0.0016$, $R^2 = 0.999$

$I4/m$ meionite: Al = 6.0(4) $<T–O>$ – 9.6(1.0)
$\sigma = 0.0029$, $R^2 = 0.989$

(2) In $I4/m$ marialite, there is no Al at the $T(1)$ site (*cf.* Sokolova *et al.* 1996).

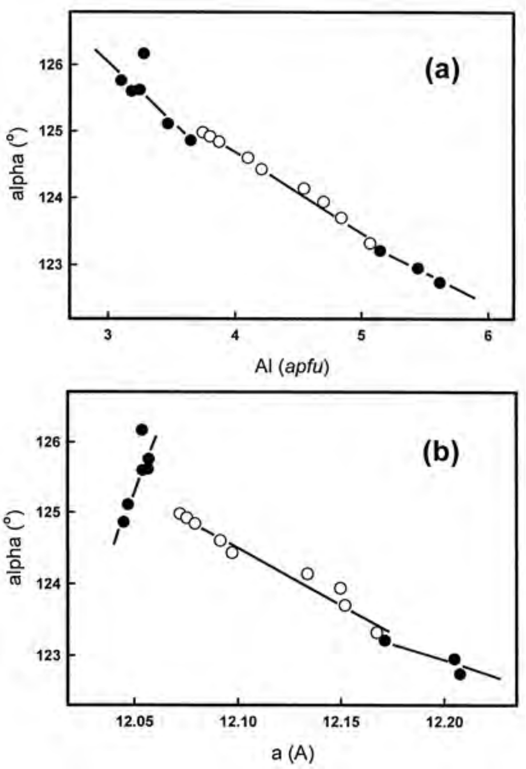

FIG. 17. Variation in α angle (see text) in the marialite–meionite series as a function of (a) total Al (*apfu*) and (b) *a* cell-parameter; legend as in Figure 6.

(3) In $P4_2/n$ scapolite, Al is strongly ordered at $T(2)$, and Si is strongly ordered at $T(3)$, but this order is never complete.

(4) The *M* cation (Na, Ca, K) is [8]-coordinated in end-member marialite and (on average) [8.5]-coordinated in end-member meionite.

(5) At the *A* site, there are four (CO_3) groups arranged about the 4 axis ($I4/m$) or $\bar{4}$ axis ($P4_2/n$) (*cf.* Papike & Stephenson 1966, Levien & Papike 1976); this arrangement is consistent across the complete series from marialite to meionite.

(6) There are also (SO_4) groups at the *A* site in some scapolites. In the $I4/m$ structure, the (SO_4) group is disordered by rotation of 90° about the central 4-fold axis, with 50% occupancy of each arrangement. In the $P4_2/n$ structure, the (SO_4) group is disordered into two orientations, but the occupancies of each arrangement are not equal (*cf.* Peterson *et al.* 1979).

ACKNOWLEDGEMENTS

This paper and its companion are dedicated to Joe Smith in recognition of his major contributions to the crystallography of rock-forming minerals.

We thank the reviewers for their comments and Editor Bob for his directions. We thank David Teertstra for samples S(10) and S(11), Alexander Zolotarev for sample S(13), Alexander Khomyakov for sample S(15), Giovanni Ferraris and Paolo Orlandi for sample S(17) from the Mineralogical Museum, Dipartimento di Scienze della Terra, Universitá di Pisa, Pisa, Italy, and Bob Ramik for sample S(18) from the Royal Ontario Museum, Toronto, Canada. FCH was supported by a Canada Research Chair in Crystallography and Mineralogy and by Major Facilities Access, Major Equipment, Equipment and Discovery Grants from the Natural Sciences and Engineering Research Council of Canada.

REFERENCES

AITKEN, B.G., EVANS, H.T., JR. & KONNERT, J.A. (1984): The crystal structure of a synthetic meionite. *Neues Jahrb. Mineral., Abh.* **149**, 309-324.

BAYLISS, P. (1987): Mineral nomenclature: scapolite. *Mineral. Mag.* **51**, 176.

BELOKONEVA, E.L., SOKOLOVA, N.V. & DOROKHOVA, G.I. (1991): Crystal structure of natural Na,Ca-scapolite – an intermediate member of the marialite–meionite series. *Sov. Phys. Crystallogr.* **36**, 828-830.

BELOKONEVA, E.L., SOKOLOVA, N.V. & URUSOV, V.S. (1993): Scapolites – crystalline structures of marialite (Me_{11}) and meionite (Me_{88}), space group as a function of composition. *Crystallogr. Rep.* **38**, 25-28.

COMODI, P., MELLINI, M. & ZANAZZI, P.F. (1990): Scapolites: variation of structure with pressure and possible role in the storage of fluids. *Eur. J. Mineral.* **2**, 195-202.

EVANS, B.W., SHAW, D.M. & HAUGHTON, D.R. (1969): Scapolite stoichiometry. *Contrib. Mineral. Petrol.* **24**, 293-305.

GRAZIANI, G. & LUCCHESI, S. (1982): The thermal behaviour of scapolites. *Am. Mineral.* **67**, 1229- 1241.

HASSAN, I. & BUSECK, P.R. (1988): HRTEM characterization of scapolite solid solutions. *Am. Mineral.* **73**, 119-134.

INTERNATIONAL TABLES FOR X-RAY CRYSTALLOGRAPHY (1992): Vol. C. Kluwer Academic Publishers, Dordrecht, The Netherlands.

KIHARA, K. (1990): An X-ray study of the temperature dependence of the quartz structure. *Eur. J. Mineral.* **2**, 63-77.

LEVIEN, L. & PAPIKE, J.J. (1976): Scapolite crystal chemistry: aluminum–silicon distributions, carbonate group disorder, and thermal expansion. *Am. Mineral.* **61**, 864-877.

LIEFTINK, D.J., NIJLAND, T.G. & MAIJER, C. (1993): Cl-rich scapolite from Ødegårdens Verk, Bamble, Norway. *Norsk Geol. Tidsskr.* **73**, 55-57.

LIN, S.B. (1975): Crystal chemistry and stoichiometry of the scapolite group. *Acta Geol. Taiwan.* **18**, 36-48.

LIN, S.B. & BURLEY, B.J. (1973a): Crystal structure of a sodium and chlorine-rich scapolite. *Acta Crystallogr.* **B29**, 1272-1278.

LIN, S.B. & BURLEY, B.J. (1973b): The crystal structure of meionite. *Acta Crystallogr.* **B29**, 2024-2026.

LIN, S.B. & BURLEY, B.J. (1973c): On the weak reflections violating body-centered symmetry in scapolites. *Tschermaks Mineral. Petrogr. Mitt.* **20**, 28-44.

LIN, S.B. & BURLEY, B.J. (1975): The crystal structure of an intermediate scapolite – wernerite. *Acta Crystallogr.* **B31**, 1806-1814.

PAPIKE, J.J. & STEPHENSON, N.C. (1966): The crystal structure of mizzonite, a calcium- and carbonate-rich scapolite. *Am. Mineral.* **51**, 1014-1027.

PAPIKE, J.J. & ZOLTAI, T. (1965): The crystal structure of a marialite scapolite. *Am. Mineral.* **50**, 641-655.

PAULING, L. (1930): The structure of some sodium and calcium alumino-silicates. *Wash. Proc. Acad. Sci.* **16**, 453-459.

PETERSON, R.C., DONNAY, G. & LE PAGE, Y. (1979): Sulfate disorder in scapolite. *Can. Mineral.* **17**, 53-61.

SCHIEBOLD, E. & SEUMEL, G. (1932): Über die Kristallstruktur von Skapolith. *Z. Kristallogr.* **81**, 110-134.

SETO, Y., SHIMOBAYASHI, N., MIYAKE, A. & KITAMURA, M. (2004): Composition and $I4/m$–$P4_2/n$ phase transition in scapolite solid solutions. *Am. Mineral.* **89**, 257-265.

SHANNON, R.D. (1976): Revised effective ionic radii and systematic studies of interatomic distances in halides and chalcogenides. *Acta Crystallogr.* **A32**, 751-767.

SHAW, D.M. (1960a): The geochemistry of scapolite. I. Previous work and general mineralogy. *J. Petrol.* **1**, 218-260.

SHAW, D.M. (1960b): The geochemistry of scapolite. II. Trace elements, petrology, and general geochemistry. *J. Petrol.* **1**, 261-285.

SHELDRICK, G.M. (1997): *SHELXL97, Program for the solution and refinement of crystal structures*. University of Göttingen, Göttingen, Germany.

SHELDRICK, G.M. (1998): *SADABS User Guide*, University of Göttingen, Göttingen, Germany.

SHERRIFF, B.L., SOKOLOVA, E.V., KABALOV YU.K., JENKINS, D.M., KUNATH-FANDREI, G., GOETZ, S., JÄGER, C. & SCHNEIDER, J. (2000): Meionite: Rietveld structure-refinement, ^{29}Si MAS and ^{27}Al SATRAS NMR spectroscopy and comments on the marialite–meionite series. *Can. Mineral.* **38**, 1201-1213.

Sherriff, B.L., Sokolova, E.V., Kabalov Yu.K., Teertstra, D.K., Kunath-Fandrei, G., Goetz, S. & Jäger, C. (1998): Intermediate scapolite: ^{29}Si MAS and ^{27}Al SATRAS NMR spectroscopy and Rietveld structure-refinement. *Can. Mineral.* **36**, 1267-1283.

Sherriff, B.L. & Teertstra, D.K. (1994): A reevaluation of the crystal chemistry and structure of the scapolite group minerals. *Int. Mineral. Assoc., 16th General Meeting* (*Pisa*), 372-373 (abstr.).

Sokolova, E.V., Gobechiya, E.R., Zolotarev, A.A. & Kabalov, Yu.K. (2000): Refinement of the crystal structures of two marialites from the Kukurt deposit of the East Pamirs. *Crystallogr. Rep.* **45**(6), 934-938.

Sokolova, E.V., Kabalov, Yu.K., Sherriff, B.L., Teertstra, D.K., Jenkins, D.M., Kunath-Fandrei, G., Goetz, S. & Jäger, C. (1996): Marialite: Rietveld structure-refinement and ^{29}Si MAS and ^{27}Al satellite transition NMR spectroscopy. *Can. Mineral.* **34**, 1039-1050.

Teertstra, D.K., Schindler, M., Sherriff, B.L. & Hawthorne, F.C. (1999): Silvialite, a new S-dominant member of the scapolite group with an Al–Si composition near the $I4/m - P4_2/n$ phase transition. *Mineral. Mag.* **63**, 321-329.

Teertstra, D.K. & Sherriff, B.L. (1996): Scapolite cell-parameter trends along the solid-solution series. *Am. Mineral.* **81**, 169-180.

Teertstra, D.K. & Sherriff, B.L. (1997): Substitutional mechanisms, compositional trends and the end-member formulae of scapolite. *Chem. Geol.* **136**, 233-260.

Ulbrich, H.H. (1973a): Structural refinement of the Monte Somma scapolite, a 93% meionite. *Schweiz. Mineral. Petrogr. Mitt.* **53**, 385-393.

Ulbrich, H.H. (1973b): Crystallographic data and refractive indices of scapolites. *Am. Mineral.* **58**, 81-92.

Zolotarev, A.A. (1993): Gem scapolites from the eastern Pamirs and some general constitutional features of scapolites. *Zap. Vser. Mineral. Obshchest.* **122**(2), 90-102 (in Russ.).

Zolotarev, A.A. (1996): Once more on isomorphic schemes and isomorphic series in the scapolite group. *Zap. Vser. Mineral. Obshchest.* **125**(1), 69-73 (in Russ.).

Received December 15, 2006, revised manuscript accepted December 1, 2008.